Torus Maps and the Problem of One-Dimensional Optical Resonator with a Quasiperiodically Moving Wall

Nikola P. Petrov[*][†]

Department of Physics

University of Texas at Austin

Austin, TX 78712

Rafael de la Llave[‡]

(Corresponding author)

Department of Mathematics

University of Texas at Austin

Austin, TX 78712

Fax (512) 471-9038

John A. Vano[§][¶]

Department of Mathematics

University of Texas at Austin

Austin, TX 78712

(Dated: September 10, 2002)

[*] Address after September 1, 2002: Department of Mathematics, University of Michigan, Ann Arbor, MI 48109–1109, USA.

[§] Address after September 1, 2002: Department of Mathematics, University of Wisconsin, Madison, WI 53706–1388, USA.

Abstract

We study the problem of the asymptotic behavior of the electromagnetic field in an optical resonator one of whose walls is at rest and the other is moving quasiperiodically (with $d \geq 2$ incommensurate frequencies).

We show that this problem can be reduced to a problem about the behavior of the iterates of a map of the d-dimensional torus that preserves a foliation by irrational straight lines. In particular, the Jacobian of this map has $(d-1)$ eigenvalues equal to 1.

We present rigorous and numerical results about several dynamical features of such maps. We also show how these dynamical features translate into properties for the field in the cavity. In particular, we show that when the torus map satisfies a KAM theorem – which happens for a Cantor set of positive measure of parameters – the energy of the electromagnetic field remains bounded. When the torus map is in a resonant region – which happens in open sets of parameters inside the gaps of the previous Cantor set – the energy grows exponentially.

PACS numbers: 05.45.-a, 42.60.Da, 02.30.Jr, 42.15.-i

†Electronic address: npetrov@math.utexas.edu

‡Electronic address: llave@math.utexas.edu

¶Electronic address: jvano@math.utexas.edu

Contents

I. INTRODUCTION

Recently, the problem of the behavior of electromagnetic fields in a one-dimensional optical resonator with a periodically moving wall has been studied intensively from both classical [1–6] and quantum [7–13] points of view. It has also been considered in the mathematics literature [14–19].

In [5], the problem of the behavior of the electromagnetic field in a cavity with one stationary boundary and one moving perfectly reflecting boundary was analyzed from the point of view of the theory of dynamical systems. The conclusion of [5] is that, if the correct boundary conditions at the mirrors are imposed, one can reformulate the problem of the behavior of the electromagnetic field in terms of a circle map determined by the motion of the wall. Then, by studying the dynamical properties of this circle map, one can draw conclusions about the asymptotic behavior of the electromagnetic field in the resonator.

In the present paper, we study a generalization of this problem to the case of a quasiperiodic motion of the mirror. We are interested in the asymptotic behavior of the electromagnetic field in the resonator. We use an approach similar to the one used in [5], and reformulate the problem in terms of certain maps of the torus. This allows us to draw conclusions about the asymptotic behavior of the field in the resonator in terms of the dynamical properties of these torus maps.

In particular, we obtain that if we consider typical families of motions described by several parameters (e.g., the amplitude of the Fourier coefficients of the motion of the boundary), then there exists an open and nonempty set of parameters for which the electromagnetic field has exponentially growing energy (this situation is called "phase locking"), and another set of parameters for which the energy remains bounded. In the case that the energy is unbounded, the electromagnetic field concentrates in pulses of exponentially decreasing width which move quasiperiodically. In the case that the energy does not grow, the derivatives of the field remain uniformly bounded for all times. Both sets of parameters interpenetrate each other. The set with bounded energy is a Cantor set and the unbounded growth lies within the gaps of this Cantor set.

We also discuss (Section V F) how these conclusions are altered if one imposes other boundary conditions (which is physically reasonable for other models such as acoustic waves in an open pipe, etc.). In Section V G we also study the time evolution of other conserved quantities of the wave equation on the whole real line (they are basically Sobolev norms). In Section V H we explain how our approach can be applied to the case of a resonator with two (quasi)periodically moving mirrors.

The torus maps that appear in our treatment of pulsating cavities have several special properties, the most striking one being that they preserve an irrational foliation (see Sec. II E and III E). This leads to several dynamical consequences, notably that there is only one nonzero Lyapunov exponent. The set of parameters for which this exponent is negative are the phase locked regions. We will give a description of these regions and will also show that, when the dynamical system is in the phase locked region, the field in the cavity has an exponentially growing energy. Moreover, we will derive a relationship between the rate of increase of the energy (the "Doppler factor") and the nonzero Lyapunov exponent.

Another region where the dynamics can be understood is a region where KAM (Kolmogorov-Arnol'd-Moser) techniques apply. In such a case, the derivatives of the electromagnetic field remain bounded and, as a consequence, the energy of the electromagnetic field remains bounded.

There may be regions in parameter space which are not covered by either of the above two descriptions. At the moment, we do not know what behavior to expect there, nor what the consequences would be for the field in the cavity.

In the analysis of the dynamics we will mention some mathematically sophisticated results and, rather than presenting proofs, we refer to places where these results can be found. The main goal of this paper is to derive the physical consequences for the problem of radiation in the cavity. It is also true that the motivation for some of the mathematical papers ([20, 21]) is precisely the derivation of the models presented here.

We present a numerical study of the phase locked regions, which, besides giving a description of the boundaries of the regions of unbounded energy, suggests several questions of a more dynamical nature.

A physical problem similar to the one studied in this article has been studied in [22], from a very different point of view.

The paper is organized as follows:

In Section II we describe the physical problem and derive a mathematical model (PDE + boundary conditions) and show how to reduce it (via the method of characteristics) to the study of a special class of torus maps. In Section III we present some mathematical results on the analysis of the torus maps – most importantly, KAM and normal hyperbolicity results. In Section IV we explore the torus maps numerically. In Section V we apply the conclusions drawn from the mathematical theory and the numerical study to the problem of the electromagnetic field in the resonator, and, in particular, we derive a simple relationship between the Lyapunov exponent of the torus map and the Doppler factor at reflection from the moving mirror. We give simple reasoning about the asymptotic behavior of the energy for the boundary conditions for the optical resonator. We conclude by discussing briefly other related problems such as the consideration of other boundary conditions, the evolution of other quantities conserved by the wave equation (basically Sobolev norms) and the adaptations needed to for the case that the two ends of the cavity are moving.

II. DERIVATION OF THE MATHEMATICAL MODEL

In this section we describe the physical model of the electromagnetic field in the resonator (Section II A), derive the boundary value problem (Section II B), explain how to solve the model using the method of characteristics (Section II C) and what mechanism is responsible for the change of the energy of the field in the cavity (Section II D). Finally, in Section II E we derive the torus map describing the evolution of the electromagnetic field.

A. Physical setup

Consider the classical (i.e., not quantized) electromagnetic field between two flat infinite perfectly reflecting mirrors, both of them perpendicular to the x-axis. Let one of the mirrors be at rest at $x = 0$ with the other mirror moving quasiperiodically, its position being given by

$$x = a(t) = \Phi(\boldsymbol{\omega} t) \ , \tag{1}$$

where the function $\Phi : \mathbb{R}^d \to \mathbb{R}$ is periodic of period 1 in each argument:

$$\begin{aligned}
&\Phi(\Xi_1, \ldots, \Xi_{j-1}, \Xi_j + 1, \Xi_{j+1}, \ldots, \Xi_d) \\
&\quad = \Phi(\Xi_1, \ldots, \Xi_{j-1}, \Xi_j, \Xi_{j+1}, \ldots, \Xi_d) \ .
\end{aligned} \tag{2}$$

For the moment, we will not need to make any assumptions on $\boldsymbol{\omega} \in \mathbb{R}^d$. In some parts of the paper, we will assume that $\boldsymbol{\omega}$ is incommensurate (see Def. III.2) or, sometimes, that it is Diophantine (Def. III.3).

The vector $\boldsymbol{\omega}$ is called the *frequency vector*. Note that our convention is to take angles modulo 1 rather than modulo 2π.

Due to the fact that only the fractional parts of Ξ_j matter due to (2), we call the fractional parts of the Ξ_j's *phases* of the motion of the mirror.

We also impose the physically natural conditions

$$a(t) = \Phi(\boldsymbol{\omega} t) \geq \Phi_{\min} > 0 \quad \forall t \in \mathbb{R} \tag{3}$$

(positive length of the resonator), and

$$|a'(t)| = |\boldsymbol{\omega} \cdot \nabla\Phi(\boldsymbol{\omega} t)| < 1 \quad \forall t \in \mathbb{R} \tag{4}$$

(the speed of the mirror does not exceed the speed of light).

In our numerical simulations we study the case of two frequencies ($d = 2$) and the map

$$\Phi(\Xi_1, \Xi_2) \ = \ \frac{\alpha}{2} + \beta \left[\sin\left(2\pi\Xi_1\right) + \gamma \sin\left(2\pi\Xi_2\right)\right] \ , \tag{5}$$

$$\boldsymbol{\omega} \ = \ (1, \sigma_{\mathrm{G}}) \ , \quad \sigma_{\mathrm{G}} \equiv \tfrac{\sqrt{5}-1}{2} \ , \tag{6}$$

with the constants α, β and γ chosen in such a way that (5) satisfies (3) and (4).

B. Derivation of the boundary value problem

In the space between the mirrors we assume plane electromagnetic waves and impose Coulomb gauge. Thus, we can take the vector potential to be of the form

$$\vec{A}(t,x) = A(t,x)\,\vec{e}_y\ ,$$

where the function $A(t,x)$ is a solution of the one-dimensional wave equation

$$A_{tt} - A_{xx} = 0\ , \quad (t,x) \in \Sigma \tag{7}$$

in the space-time domain

$$\Sigma \equiv \{\,(t,x) \mid t \geq 0,\ x \in [t, a(t)]\,\}\ . \tag{8}$$

The boundary conditions come from the fact that the component of the electric field tangent to the mirrors vanishes at the mirrors in the rest frame of the corresponding mirror. After a Lorentz transform to the laboratory frame, this yields the boundary conditions [5]

$$A_t(t,0) \ = \ 0\ , \quad t \geq 0 \tag{9}$$

$$A_t(t,a(t)) + a'(t)\,A_x(t,a(t)) \ = \ 0\ , \quad t \geq 0\ . \tag{10}$$

Initial conditions

$$A(0,x) = \psi_1(x)\ , \quad A_t(0,x) = \psi_2(x)\ , \quad x \in [0,a(0)] \tag{11}$$

must be imposed as well.

We call attention to the fact that the physically natural boundary conditions (9), (10) are not the usual Dirichlet or Neumann boundary conditions and are the only boundary conditions compatible with Lorentz covariance. The boundary conditions (9), (10) are exactly the boundary conditions that make the method of characteristics work in a straightforward manner (see Sec. II C). Note that the boundary conditions (9), (10) can be understood as vanishing of the derivative of $A(t,x)$ in the direction tangent to the world line of the mirrors. Hence, (9), (10), are implied by the Dirichlet boundary conditions $A(t,0) = A(t,a(t)) = 0$.

Remark II.1 *Even though the boundary conditions* (9), (10) *are the only physically reasonable ones for the electromagnetic field, there are other physical interpretations of the* *wave equation for which other boundary conditions may be appropriate. For example, in the problem of the pressure field in a pipe with open ends and with variable length, Neumann boundary conditions,*

$$u_x(t,0) = u_x(t,a(t)) = 0 \ , \tag{12}$$

are appropriate. (See the discussion of the boundary conditions and the radiation pressure in the classical papers [23–26].) The role of the boundary conditions in the translation from the dynamical properties of a map to the properties of the field in the cavity is studied in greater detail in Section V F.

C. Method of characteristics in a spatially bounded domain

If there are no spatial boundaries, i.e., if $\Sigma = [0,\infty) \times \mathbb{R}$, the well-known method of characteristics [27–29] implies that $A(t,x)$ can be written as

$$A(t,x) = \Psi^-(x_0^-) + \Psi^+(x_0^+) \ , \tag{13}$$

where $x_0^\pm \equiv x \pm t$ and

$$\Psi^\pm(s) \equiv \frac{1}{2}\left[\psi_1(s) \pm \int_\zeta^s \psi_2(s')ds'\right] \tag{14}$$

(ζ is an arbitrary constant with the same value for Ψ^+ and Ψ^-).

The meaning of (13) is simple: the value of $A(t,x)$ is a superposition of the values of two functions – one being constant along the characteristics $\{x - t = \text{const}\}$ (corresponding to rays "propagating to the right"), and the other being constant along the characteristics $\{x + t = \text{const}\}$ (rays "propagating to the left").

In the presence of spatial boundaries this method can be modified so that the function $A(t,x)$ satisfies the boundary conditions (9), (10). The characteristics in this case are piecewise straight lines that always make an angle of 45° with the t axis and the functions $\Psi^\pm$ are constant on these characteristics and change sign at reflection from a mirror. A simple argument (see [5]) shows that (13) should be replaced by

$$A(t,x) = (-1)^{N_-}\Psi^-(x_0^-) + (-1)^{N_+}\Psi^+(x_0^+) \ , \tag{15}$$

where $N_\mp$ are the number of reflections of the characteristic $\gamma^\mp$ on the way back from (t,x) to $(0,x_0^\mp)$; the meaning of the notations is clear from Figure 1(a).

It can be shown that the solution constructed with this algorithm satisfies the boundary conditions (see [5]).

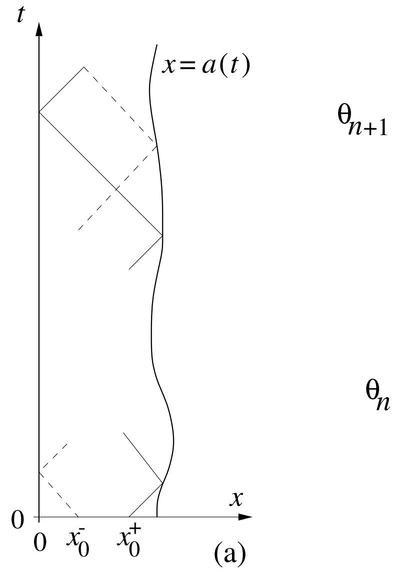

FIG. 1: (a) Characteristics of the wave equation. (b) Times of reflection.

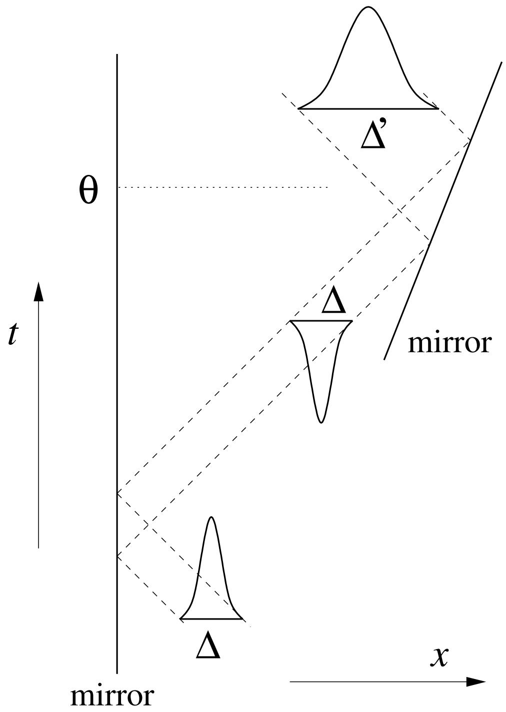

FIG. 2: Reflection of a narrow wave packet.

D. Mechanism and rate of the energy change in the cavity with moving boundaries

To understand the mechanism of the energy change, consider a very narrow wave packet that is reflected from the moving mirror at time θ, as shown in Figure 2. From the geometry of the space-time diagram, one can easily observe that if the width of the wave packet before reflection is Δ, after reflection it will be

$$\Delta' \approx \mathcal{D}(\theta)\,\Delta\ , \tag{16}$$

where

$$\begin{aligned} \mathcal{D}(\theta) &\equiv \frac{1-a'(\theta)}{1+a'(\theta)} \\ &= \frac{1-\boldsymbol{\omega}\cdot\nabla\Phi(\boldsymbol{\omega}\theta)}{1+\boldsymbol{\omega}\cdot\nabla\Phi(\boldsymbol{\omega}\theta)} \end{aligned} \tag{17}$$

is the Doppler factor. At the same time, the vector potential will only flip sign. Thus, the absolute values of the partial derivatives of A will change by a factor of $\mathcal{D}(\theta)$, and at the same time the support Δ will change by a factor of $\mathcal{D}(\theta)^{-1}$, so the energy of the wave packet will increase by a factor $\mathcal{D}(\theta)$ at reflection:

$$\begin{aligned} \mathcal{E}_{\text{after reflection}} &\approx \int_{\Delta'} dx'\,\tfrac{1}{8\pi}(\vec{E}'^2+\vec{B}'^2) \\ &= \int_{\Delta'} dx'\,\tfrac{1}{8\pi}({A'_t}^2+{A'_x}^2) \\ &= \frac{1}{\mathcal{D}(\theta)}\int_{\Delta} dx\ \left[\mathcal{D}(\theta)^2\tfrac{1}{8\pi}({A_t}^2+{A_x}^2)\right] \\ &= \mathcal{D}(\theta)\,\mathcal{E}_{\text{before reflection}}\ . \end{aligned} \tag{18}$$

E. Derivation of the torus map

The asymptotic behavior of the characteristics – and hence the electromagnetic field – can be studied quite effectively by the following device.

We denote by $\mathbf{\Pi}:\mathbb{R}^d\to\mathbb{T}^d\equiv\mathbb{R}^d/\mathbb{Z}^d$ the projection

$$\boldsymbol{\xi}\equiv\mathbf{\Pi}(\mathbf{\Xi})=(\Xi_1 \bmod 1,\ \ldots,\ \Xi_d \bmod 1)\ . \tag{19}$$

This projection appears naturally in the study of quasiperiodic motions since, due to (2), the state of the moving mirror is completely characterized by the phase $\boldsymbol{\xi}\equiv\mathbf{\Pi}(\boldsymbol{\omega}t)$ which determines not only the position $a(t)=\Phi(\boldsymbol{\omega}t)$, but also the derivatives $a'(t)$ and all future and past phases at reflection.

We adopt the convention of referring to the objects in $\mathbb{T}^d$ as the *phases* and denote them by lower case boldface letters, while the objects in $\mathbb{R}^d$ will be denoted by uppercase boldface letters.

Let θ_n be the time of the n^{th} reflection of a particular characteristic ("ray") from the moving mirror. We will see that there is a very explicit expression that gives θ_{n+1} in terms of θ_n. From Figure 1(b), it is clear that

$$\theta_{n+1} - a(\theta_{n+1}) = \theta_n + a(\theta_n) \ . \tag{20}$$

Let $\mathbf{G}$ be the map that gives $\boldsymbol{\omega}\theta_{n+1}$ in terms of $\boldsymbol{\omega}\theta_n$:

$$\mathbf{G} : \mathbb{R}^d \to \mathbb{R}^d : \boldsymbol{\omega}\theta_n \mapsto \boldsymbol{\omega}\theta_{n+1} \ .$$

Multiplying (20) by $\boldsymbol{\omega}$ and taking into account (1), we obtain an expression for $\mathbf{G}$:

$$\mathbf{G} = (\mathrm{Id} - \boldsymbol{\omega}\Phi)^{-1} \circ (\mathrm{Id} + \boldsymbol{\omega}\Phi) \ . \tag{21}$$

If the mirror is moving periodically with period 1, (21) becomes

$$G = (\mathrm{Id} - a)^{-1} \circ (\mathrm{Id} + a) \ . \tag{22}$$

Remark II.2 *Due to the condition* (4), $\mathrm{Id} - \boldsymbol{\omega}\Phi$ *is always invertible, so* $\mathbf{G}$ *(and the map* $\mathbf{g}$ *defined below) are well-defined.*

Now let us note that due to (2), we do not need to know the Ξ_j's, but only their fractional parts – the phases $\xi_j = \Xi_j \bmod 1 \in \mathbb{T}^1$. Because of this, we define the map $\mathbf{g} : \mathbb{T}^d \to \mathbb{T}^d$ as follows. Let $\boldsymbol{\xi} \in \mathbb{T}^d$ and $\boldsymbol{\Xi} \in \mathbb{R}^d$ be a lift of $\boldsymbol{\xi}$, i.e., $\xi_j = \Xi_j \bmod 1$ for each $j = 1, \ldots, d$. Then we define the map

$$\mathbf{g} \equiv (g_1, g_2, \ldots, g_d) : \mathbb{T}^d \to \mathbb{T}^d$$

by

$$g_j(\boldsymbol{\xi}) \equiv G_j(\boldsymbol{\xi}) \bmod 1 \ . \tag{23}$$

In mathematical language, $\mathbf{g}$ can be defined as the map such that

$$\mathbf{g} \circ \boldsymbol{\Pi} = \boldsymbol{\Pi} \circ \mathbf{G} \ , \tag{24}$$

where $\boldsymbol{\Pi}$ is defined by (19). We will call $\mathbf{g}$ the *phase advance map.*

Note also that $\mathbf{G}$ has the form

$$\mathbf{G}(\boldsymbol{\Xi}) = \boldsymbol{\Xi} + \Gamma(\boldsymbol{\Xi})\boldsymbol{\omega} \ , \tag{25}$$

where Γ is a strictly positive real-valued function (since the length of the cavity is bounded from below by $\Phi_{\min} > 0$ (3)).

The physical interpretation of $\Gamma(\boldsymbol{\Xi})$ is the time spent between the reflection from the moving mirror at moment t when the phase of the mirror's motion is $\boldsymbol{\xi} = \boldsymbol{\Pi}(\boldsymbol{\omega} t)$, and the next reflection from the moving mirror; here $\boldsymbol{\xi} = \boldsymbol{\Pi}(\boldsymbol{\Xi})$.

Remark II.3 *Torus maps satisfying* (25) *are a very particular class of torus maps, as explained in Sec. III E.*

Maps of the type (25) *have also appeared in the mathematical literature. The thesis [30] contains a study of maps of the form* (25) *that are also area-preserving. Reparametrizations of irrational flows on the torus are also of the form* (25)*. We note, however, that there are many maps of the form* (25) *which are not reparametrizations of irrational flows. The papers [31, 32] construct reparametrizations of irrational flows on the torus (hence maps of the form* (25)*) with very complicated ergodic properties which we will not discuss further in this paper.*

A particular case of the above construction is when $a(t) \equiv \bar{a}$, i.e., the right mirror is at rest at a distance $\bar{a}$ from the left one. In this case, (21) reduces to

$$G(\boldsymbol{\Xi}) = \boldsymbol{\Xi} + 2\bar{a}\boldsymbol{\omega} \ .$$

This particularly simple case is what we will treat as the unperturbed case in the KAM theory of Sec. III F.

Note that, even if one can think of the variable n as a discrete time – indeed this is the notion used very often in dynamics–, this is not the physical time.

Given a characteristic, we introduce the *"average transit time"*

$$T = \lim_{n\to\infty} t_n/n. \tag{26}$$

Note that we can write $T = \lim_n \frac{1}{n} \sum_{i=0}^{n-1} (t_{i+1} - t_i)$ or, denoting $\Delta(\mathbf{g}^i(\boldsymbol{\xi})) = t_{i+1} - t_i$, the time between reflections and taking into account that it is a function of the phases at the i^{th} reflection, we have

$$T = \lim_n \frac{1}{n} \sum_{i=0}^{n-1} \Delta(\mathbf{g}^i(\boldsymbol{\xi}))$$

The average above exists by Birkhoff ergodic theorem almost everywhere for any invariant measure.

Actually, for the situations we will be interested in later – the regions in which we have KAM or attracting invariant circles with an irrational rotation – it turns out that there is only an invariant measure. In such a case, the limit above exists everywhere and moreover is reached uniformly. See [33].

III. ANALYSIS OF THE TORUS MAP

In this section we give a short exposition of the facts from the theory of torus maps necessary for the analysis of the torus map $\mathbf{g}$ (23) and explain some rigorous results for torus maps. In Sec. IV we present some numerical results. Sec. V contains a discussion of the interpretations of the rigorous and numerical results of Sec. III and Sec. IV for the cavity problem.

This section is organized as follows. First, In Sections III A,III B, III C we recall several standard results and notations. The core of our analysis is the KAM theory developed in Sec. III F and the theory of Lyapunov exponents is discuss in Sec. III G. In Section III H we study in detail a configuration that we encounter often in practice.

We point out that the literature on the dynamical properties of torus maps is quite extensive both in the mathematical and the physical literature. Torus maps appear in ergodic theory [34], in the description of systems of coupled oscillators [35], play a central role in the Ruelle-Takens-Newhouse scenario for transition to turbulence [36] (see also [37, 38]), Schrödinger's equation with a quasiperiodic potential [39–41], Hill's equation with a quasiperiodic forcing [42]; bifurcations of quasiperiodic tori have been studied in detail in [43].

A. Rotation set

A basic concept in the theory of torus maps is the concept of the rotation set of the orbits of a map.

Let $\mathbf{g}$ be a torus map, and $\mathbf{G}$ be a *lift* of $\mathbf{g}$, i.e., a map of $\mathbb{R}^d$ to itself that is related to $\mathbf{g}$ by (24) (any torus map has infinitely many lifts, differing by an integer vector $\mathbf{p} \in \mathbb{Z}^d$).

Definition III.1 *Let* $\mathbf{G}$ *be a lift of the torus map* $\mathbf{g}$ *and let* $\boldsymbol{\xi} \in \mathbb{T}^d$*, and* $\Xi \in \mathbb{R}^d$ *be any lift of* $\boldsymbol{\xi}$*, (i.e.,* $\mathbf{\Pi}(\Xi) = \boldsymbol{\xi}$*). The* rotation set $\boldsymbol{\tau}(\boldsymbol{\xi}, \mathbf{g})$ *of the point* $\boldsymbol{\xi}$ *under the map* $\mathbf{g}$ *is the set of* *the accumulation points of*

$$\boldsymbol{\Pi}\left(\frac{\mathbf{G}^n(\Xi)-\Xi}{n}\right)\ , \quad n\in\mathbb{N}\ . \tag{27}$$

If the limit

$$\boldsymbol{\tau}(\boldsymbol{\xi},\mathbf{g})\equiv\boldsymbol{\Pi}\left(\lim_{n\to\infty}\frac{\mathbf{G}^n(\Xi)-\Xi}{n}\right)\ , \tag{28}$$

exists (i.e., if $\boldsymbol{\tau}(\boldsymbol{\xi},\mathbf{g})$ *consists of one point), then it is called the* rotation vector *of* $\boldsymbol{\xi}$ *under* $\mathbf{g}$*.*

We denote the rotation vector (if it exists) of a map $\mathbf{g}$ *by* $\boldsymbol{\rho}(\mathbf{g})$*.*

Remark III.1 *The rotation set is always nonempty, compact and connected [44], and it does not depend on the choice of a lift of* $\mathbf{g}$*.*

Remark III.2 *For circle maps* ($d=1$)*, the limit in the right-hand side of* (28) *always exists and does not depend on* $\boldsymbol{\xi}$ *[45, Chap. 11]. In other words, the rotation set consists of only one number called the* rotation number*.*

Remark III.3 *When* $d>1$*, the structure of the rotation set could be very complicated for a generic map of the torus. See, for example [46] and references there.*

One could hope that for maps of the form (25)*, it was possible to develop a more systematic theory. Using KAM theory, it is possible to show that for families of maps close to rotations and satisfying suitable non-degeneracy assumptions there are large measure sets parameters for which the rotation set consists only of one point. See [20], [22] (a summary of the main results of [20] are in Sec. III F). See also [30] for a proof of existence of a rotation vector for maps of the form* (25) *under the hypothesis of area preservation.*

B. Arithmetic properties of vectors

Below, we summarize some standard number-theoretic properties of vectors in $\mathbb{R}^d$ that are important for our exposition.

Definition III.2 *A vector* $\boldsymbol{\rho}\in\mathbb{T}^d$ *is called:*

(A) incommensurate *if for any* $\mathbf{m}\in\mathbb{Z}^d$ *and* $k\in\mathbb{Z}$ *the equality*

$$\mathbf{m}\cdot\boldsymbol{\rho}=k \tag{29}$$

implies that $\mathbf{m}=\mathbf{0}$*,* $k=0$*;*

(B) commensurate *if* (29) *holds for some* $\mathbf{m} \in \mathbb{Z}^d \setminus \{\mathbf{0}\}$ *and* $k \in \mathbb{Z} \setminus \{0\}$;

(B)$_1$ rational *if* $\boldsymbol{\rho} = \mathbf{p}/q$ *for some* $\mathbf{p} \in \mathbb{Z}^d$, $q \in \mathbb{N}$.

Remark III.4 *Obviously, all rational vectors are commensurate.*

An important concept needed for the KAM-type theorems for torus maps is the following.

Definition III.3 *A vector* $\boldsymbol{\rho} \in \mathbb{R}^d$ *is* Diophantine *if there exist constants* $C > 0$, $\nu \geq d$ *such that*

$$|\mathbf{m} \cdot \boldsymbol{\rho} - k| \geq \frac{C}{|\mathbf{m}|^\nu} \tag{30}$$

for each $\mathbf{m} \in \mathbb{Z}^d \setminus \{\mathbf{0}\}$, $k \in \mathbb{Z}$ *(here* $|\mathbf{m}| \equiv \sum_{j=1}^d |m_j|$*); we will denote this by* $\boldsymbol{\rho} \in D_{C,\nu}$.

The vector $\boldsymbol{\omega} \in \mathbb{R}^d$ *is called* Diophantine affine *if it satisfies*

$$|\mathbf{m} \cdot \boldsymbol{\rho}| \geq \frac{C}{|\mathbf{m}|^\nu}\ , \tag{31}$$

for each $\mathbf{m} \in \mathbb{Z}^d \setminus \{\mathbf{0}\}$.

Remark III.5 *Note that all Diophantine vectors are incommensurate. Also, all Diophantine vectors are Diophantine affine.*

If $\boldsymbol{\rho} \in \mathbb{R}^d$ *is Diophantine affine, so is* $t\boldsymbol{\rho}$ *for any* $t \in \mathbb{R} \setminus \{0\}$. *On the other hand, the set of Diophantine vectors is totally disconnected.*

Remark III.6 *Given a commensurate* $\boldsymbol{\rho}$, *the set*

$$\mathcal{R}_{\boldsymbol{\rho}} := \{\mathbf{m} \in \mathbb{Z}^d \,|\, \boldsymbol{\rho} \cdot \mathbf{m} \in \mathbb{Z}^d\}$$

is a $\mathbb{Z}$*-module (i.e.,* $\mathbf{m}_1, \mathbf{m}_2 \in \mathcal{R}_{\boldsymbol{\rho}}$, $l \in \mathbb{Z}$ *imply* $\mathbf{m}_1 + \mathbf{m}_2 \in \mathcal{R}_{\boldsymbol{\rho}}$, *and* $l\mathbf{m}_1 \in \mathcal{R}_{\boldsymbol{\rho}}$*). The dimension of* $\mathcal{R}_{\boldsymbol{\rho}}$ *is the order of resonance of* $\boldsymbol{\rho}$ *(i.e., the number of independent relations of the form* (29) *satisfied by* $\boldsymbol{\rho}$*).*

Remark III.7 *It is well known that the set of Diophantine vectors of exponent* ν *is of full measure in* $\mathbb{R}^d$ *when* $\nu > d+1$, *and empty when* $\nu < d+1$ *(see [47]).*

Remark III.8 *For* $\boldsymbol{\omega} \in \mathbb{R}^d$ *which is Diophantine affine (i.e., satisfies* (31)*), the set*

$$\mathcal{A} := \{t \in \mathbb{R} \,|\, t\boldsymbol{\omega} \text{ is Diophantine}\}$$

is of full measure in the real line (see [20] for the argument).

C. Translations on the torus

The simplest example of a torus map is the translation $\mathbf{t}_{\boldsymbol{\eta}}$ ($\boldsymbol{\eta} \in \mathbb{T}^d$), whose lift is given by

$$\mathbf{T}_{\boldsymbol{\eta}}(\boldsymbol{\Xi}) = \boldsymbol{\Xi} + \boldsymbol{\eta} \ .$$

Each orbit of $\mathbf{t}_{\boldsymbol{\eta}}$ has rotation vector equal to $\boldsymbol{\eta}$.

Depending on the properties of the rotation vector $\boldsymbol{\rho} \in \mathbb{R}^d$, we have:

(a) If $\boldsymbol{\rho}$ is incommensurate, then the orbit of each $\boldsymbol{\xi} \in \mathbb{T}^d$ is dense in $\mathbb{T}^d$. In fact, Weyl's theorem [45, Theorem 4.2.1] says that the only $\mathbf{t}_{\boldsymbol{\eta}}$-invariant measure is the Lebesgue measure.

(b) If $\boldsymbol{\rho}$ is commensurate but not rational, each orbit is dense on a d'-dimensional torus ($0 < d' < d$), where $d - d'$ is the order of the resonance.

Clearly, such d'-dimensional tori are invariant, disjoint, and cover $\mathbb{T}^d$. Hence, the study of the dynamics in $\mathbb{T}^d$ can be reduced to the study of the dynamics on each of the $\mathbb{T}^{d'}$.

For example, if $\boldsymbol{\rho} = (\frac{1}{3}, \frac{2}{3}, \sqrt{2})$, then (29) is satisfied by the 2-parameter family $\mathbf{m} = (3a, 3b, 0)$, $k = a + 2b$, $(a, b) \in \mathbb{Z}^2 \setminus \{(0, 0)\}$, hence $\mathbb{T}^3$ in this case is foliated by the orbits each of which is dense in a torus of dimension $d' = 1$; if $\mathbb{T}^3$ is visualized as the unit cube (with the corresponding sides identified), then the invariant one-dimensional tori are parallel to the ξ_3-axis.

(c) If $\boldsymbol{\rho}$ is rational, say $\boldsymbol{\rho} = \mathbf{p}/q \in \mathbb{Q}$, then for the lift $\boldsymbol{\Xi}$ of any $\boldsymbol{\xi} \in \mathbb{T}^d$, we have $\mathbf{G}^q(\boldsymbol{\Xi}) = \boldsymbol{\Xi} + \mathbf{p}$, therefore, each $\boldsymbol{\xi} \in \mathbb{T}^d$ is *periodic* of period q: $\mathbf{g}^q(\boldsymbol{\xi}) = \boldsymbol{\xi}$.

D. The particular case of a circle map

The simplest case of torus maps are the maps of the circle $\mathbb{T}^1$, which in the context of the physical problem at hand correspond to the case of periodic motion of the mirror. This case was treated in detail in our paper [5], where we collected the necessary definitions and theorems from the theory of circle maps, so we refer the reader to that paper and give here a very brief summary of the results in this case (for a detailed exposition see, e.g., [45, Chap. 11, 12], [48], and especially [49]).

The rotation set (27) of the circle map $g : \mathbb{T}^1 \to \mathbb{T}^1$ consists of a single point $\tau(g) \in \mathbb{T}^1$ called the *rotation number* of the map. In this case $\tau(g)$ does not depend on the lift and the point we iterate. Depending on whether $\tau(g)$ is rational or not, the following possibilities exist.

- If $\tau(g) = \frac{p}{q} \in \mathbb{Q}$, then there exist a periodic point $\boldsymbol{\xi}^*$ of period q, such that $\mathbf{G}^q(\boldsymbol{\xi}^*) = \boldsymbol{\xi}^* + p$.
- If $\tau(g) \notin \mathbb{Q}$, then the orbit of each point is dense in $\mathbb{T}^1$ or in some Cantor set. The latter possibility cannot occur if g is C^2.

If $\tau(g)$ is Diophantine and g is smooth enough, then the following theorem holds (originally a similar theorem was proved by Arnol'd and later it was significantly improved by Moser; global versions of it are due to Herman, Yoccoz, and the version given here is due to Katznelson and Ornstein [50]; for references and fuller discussion from the point of view of applications to this problem see, e.g., [5]).

Theorem III.1 *Let g be a C^k circle diffeomorphism with rotation number $\tau(g) \in D_{C,\nu}$, and $k > \nu + 1$. Then, the homeomorphism h that conjugates g with $t_{\tau(g)}$ is a diffeomorphism of class $C^{k-\nu-\epsilon}$ for any $\epsilon > 0$.*

Let $\{g_\alpha\}_{\alpha \in A}$ be a 1-parameter family of circle homeomorphisms such that $G_\alpha(\Xi)$ is increasing in the parameter α for every $\Xi \in \mathbb{R}$, e.g., the famous Arnol'd circle map,

$$g_\alpha(\xi) = (\xi + \alpha + \beta \sin 2\pi\xi) \bmod 1 \tag{32}$$

with $|\beta| \leq \frac{1}{2\pi}$. (Note that (32) is a particular case of (5) with $\gamma = 0$.) Then the rotation number $\tau(g_\alpha)$ as a function of α is a continuous function and the following facts hold:

- if $\tau(g_{\alpha'}) \notin \mathbb{Q}$, then the function $\alpha \mapsto \tau(g_\alpha)$ is strictly increasing locally at α';
- if $\tau(g_{\alpha'}) \in \mathbb{Q}$, then (generically) $\alpha \mapsto \tau(g_\alpha)$ is locally constant, i.e., for each α'' close enough to α', $\tau(g_{\alpha''}) = \tau(g_{\alpha'})$. The local constancy of $\alpha \to \tau(g_\alpha)$ is known as *phase (frequency, mode) locking.*

Note that since $\tau(g_\alpha)$ is a continuous function of α, it has to go through the dense set of rational numbers as α changes. For a generic family, this means that there is a dense set of intervals where $\tau(g_\alpha)$ is constant as a function of α. Functions of this type are called *devil's staircases.*

Let us consider the example (32) and denote by $\mathcal{I}_{p/q} \subset [0,1]$ the interval of values of α for which $\tau(g_\alpha) = \frac{p}{q} \in [0,1]$ (p, $q \in \mathbb{N}$). i.e., for which g_α is phase locked. Then the Lebesgue measure $m(\mathcal{I})$ of the union $\mathcal{I}$ of all such intervals is 0 for $\beta = 0$, has value strictly between 0 and 1 for $|\beta| \in (0, \frac{1}{2\pi})$, and is equal to 1 for $|\beta| = \frac{1}{2\pi}$. When $\mathcal{I}$ has full Lebesgue measure ($m(\mathcal{I}) = 1$), the devil's staircase is called *complete*. Note that for the family (32), this happens exactly when g_α loses its invertibility (namely, $g'_\alpha(\frac{1}{2}) = 0$); see [51] for numerical and [52, 53] for analytical results in this direction.

A question we are going to study numerically in Sec. IV is whether adding to g_α a small perturbation with irrational frequency (which in the notations of Sec. II A corresponds to small γ and incommensurate $\boldsymbol{\omega}$) destroys the phase locking and exactly how this happens.

E. Torus maps preserving a foliation

Because of (25), the maps of the torus we have derived in Sec. II E are of a very special nature. The main feature is that a straight line with direction $\boldsymbol{\omega}$ is transformed by $\mathbf{G}$ into itself. In mathematical terms this is described by saying that the maps preserve each of the leaves of $\mathcal{F}_{\boldsymbol{\omega}}$, the one dimensional foliation with direction $\boldsymbol{\omega}$. Indeed, if $\boldsymbol{\Xi} = \widetilde{\boldsymbol{\Xi}} + s\boldsymbol{\omega}$, then

$$\mathbf{G}(\boldsymbol{\Xi}) = \mathbf{G}(\widetilde{\boldsymbol{\Xi}} + s\boldsymbol{\omega}) = \widetilde{\boldsymbol{\Xi}} + s\boldsymbol{\omega} + \Gamma(\boldsymbol{\Xi})\boldsymbol{\omega} \ . \tag{33}$$

Preserving of each of the leaves is somewhat stronger then preserving the foliation (which requires only that a leaf is mapped into another leaf). The preservation of the leaves of the foliation is a very severe restriction on the maps $\mathbf{g}$ of interest for us. Hence, phenomena typical in the class of all torus maps, may not be present in our case. Similarly, phenomena that are persistent in our family man not be persistent in the case of general torus maps.

Furthermore, it is important to realize that not all the maps of the form (25) can be realized as maps arising from an oscillating cavity. Already for $d = 1$, one can find examples of this situation in [5, Section II.E]. Corresponding to this, families corresponding to generic choices of the motion of the boundary lead to families of torus maps which have non-generic properties even among the class of maps of the form (25). As we will see in the corresponding sections, cavity maps are more degenerate for KAM theory than the typical families of foliation preserving maps.

As we will discuss in Section IV D, the width of the Arnol'd tongues is different in the maps arising from the cavity than those from generic maps.

Of course, all the general results for maps as in (25) will apply to resonant cavity maps. On the other hand, results about "genericity" or "universality" may not remain valid if one changes the context in which they are discussed.

The existence of a preserved foliation implies that the rotation set is a rotation interval parallel to $\boldsymbol{\omega}$.

In the physical problem at hand, we will study only the case of an incommensurate $\boldsymbol{\omega}$, because in the case of a commensurate (but not rational) $\boldsymbol{\omega}$ we can study the dynamics restricted to the d'-dimensional tori invariant under the torus map.

If $\boldsymbol{\omega}$ is incommensurate – which in the case $d = 2$ simply means that ω_1 and ω_2 are rationally independent, – each line of the foliation $\mathcal{F}_{\boldsymbol{\omega}}$ is dense when projected ("folded back") to the torus $\mathbb{T}^d$ (see case (b) in Section III C).

We also note that since $\boldsymbol{\omega}$ is incommensurate and $\Gamma(\Xi)$ (defined in (25)) is bounded away from 0, the torus map $\mathbf{g}$ cannot have any periodic points. (Observe that the line $\boldsymbol{\xi} + \boldsymbol{\omega} t$ is mapped to itself. Since Γ is positive, the motion on this line is monotone. Because $\boldsymbol{\omega}$ is incommensurate, two different points on the line correspond to two different points on the torus.) This absence of periodic points implies very severe restrictions on the dynamics of the map.

Remark III.9 *The absence of periodic points if quite important for our examples. Prof. R. Perez-Marco has communicated to us an example due to P. Le Calvez of a map of the form* (25)*, which has a periodic orbit and for which the rotation set is not a point. We do not know whether such examples exist for maps with* Γ *bounded away from zero.*

F. KAM theory

Due to the simplicity of the translations on the torus, it is useful to know whether a general torus map is "equivalent" to a translation (up to a change of variables).

As we will see later in Lemma V.2, the fact that the torus maps appearing in the cavity problem are smoothly equivalent to a rotation has important consequences for the behavior in time of the the electromagnetic field, in particular for the growth of the energy.

The formal definition of equivalence is the following.

Definition III.4 *The torus maps* $\mathbf{g} : \mathbb{T}^d \to \mathbb{T}^d$ *and* $\mathbf{g}' : \mathbb{T}^d \to \mathbb{T}^d$ *are* (topologically, C^r, analytically) conjugate *if there exists a (continuous,* C^r*, analytic) map* $\mathbf{h} : \mathbb{T}^d \to \mathbb{T}^d$ *with a (continuous,* C^r*, analytic) inverse such that*

$$\mathbf{g} = \mathbf{h}^{-1} \circ \mathbf{g}' \circ \mathbf{h} \ . \tag{34}$$

We note that if two maps are topologically conjugate, then the rotation sets (Def. III.1) of the two maps are the same.

Simplifying somewhat, the main result of standard KAM theory is as follows:

Given any Diophantine vector $\boldsymbol{\omega}_0$ and a family of maps $\mathbf{f}^\lambda$ that depends on the d-dimensional parameter λ, satisfies some non-degeneracy conditions (see below), and is close to the translation $\mathbf{t}_{\boldsymbol{\omega}_0}$, we can find a Cantor set $\mathcal{C}$ of (Diophantine) frequencies such that for each $\boldsymbol{\omega} \in \mathcal{C}$ we can find a parameter value $\lambda(\boldsymbol{\omega})$ (which depends on $\boldsymbol{\omega}$) such that the map $\mathbf{f}^{\lambda(\boldsymbol{\omega})}$ is smoothly conjugate to the translation by the vector $\boldsymbol{\omega}$.

The degree of smoothness of the conjugacy depends on the degree of smoothness of the maps and the Diophantine exponent of $\boldsymbol{\omega}_0$.

Theorems on stability of translations under these hypotheses can be found in [49, 54–56]. A pedagogical exposition of these and other KAM theorems can be found in [47].

Remark III.10 *The reason why the standard KAM theory needs a d-dimensional parameter* $\boldsymbol{\lambda}$ *is to be able to adjust the frequency change due to the perturbation. For example, the translation* $\mathbf{t}_{\boldsymbol{\omega}_0+\boldsymbol{\Delta}}$ *cannot be conjugated to* $\mathbf{t}_{\boldsymbol{\omega}_0}$ *no matter how small* $\boldsymbol{\Delta}$ *is. The problem of lack of parameters is discussed in [57, Section V.4]. For recent developments of the problem of lack of parameters see [47, 58].*

A precise definition of the non-degeneracy assumption in the standard KAM theory is that the function

$$\boldsymbol{\varphi}(\boldsymbol{\lambda}) \equiv \int_{\mathbb{T}^d} \left[\mathbf{f}^{\boldsymbol{\lambda}}(\boldsymbol{\xi}) - \boldsymbol{\xi}\right] \, d\boldsymbol{\xi} \tag{35}$$

satisfies

$$\det D\boldsymbol{\varphi}(\mathbf{0}) \neq 0 \ . \tag{36}$$

More geometrically, we require that $D\boldsymbol{\varphi}(\mathbf{0})$ has full range.

When the nondegeneracy assumption (36) is satisfied, by adjusting the parameters one can make sure that the rotation vector is kept at the value we want.

Another problem considered in KAM theory is estimating the measure of the set of parameters for which there exists a conjugacy between $\mathbf{f}^{\boldsymbol{\lambda}}$ and a rotation. This is particularly relevant for our applications since the measure of the set of parameters relates to the observability of the phenomena. A positive (or large) measure of parameters will indicate that, picking parameter values at random, there is a (good) chance of observing the phenomena.

Unfortunately, the standard results of KAM theory do not apply for the maps of the form (25) appearing in the quasiperiodic cavity problem.

There are three reasons for this: one is that, KAM theory does not apply straightforwardly to maps of the form (25), the function $\boldsymbol{\varphi}$ defined in (35) has one dimensional range (in the direction of $\boldsymbol{\omega}$). Hence $D\boldsymbol{\varphi}(\boldsymbol{\lambda})$ has range contained in a one dimensional vector space.

As a second difficulty in our situation, we note that the parameters λ that appear in the problem (5), (6) are 1-dimensional rather than d-dimensional as required by standard KAM theory. Hence, we are considering one parameter families of maps of the form (25).

Finally, we note that the families of maps that appear in the resonant cavity problem are also rather specialized in the class of maps of the form (25). As we see below, families of maps of the form (21), which appear naturally in the study of the cavity are more degenerate than the general maps of the form (25).

More explicitly, if we consider a system with the motion of the wall being a small perturbation of a constant, i.e., $\Phi(\Xi) = \frac{\alpha}{2} + \lambda b(\Xi)$ (cf. (5), (6)), then we have for small λ

$$\mathbf{G}^{\lambda}(\Xi) = \Xi + \alpha\boldsymbol{\omega} + \lambda\left[-b(\boldsymbol{\xi} + \tfrac{\alpha}{2}\boldsymbol{\omega}) + b(\boldsymbol{\xi})\right] + O(\lambda^2) \,. \tag{37}$$

Since $\int_{\mathbb{T}^d}[-b(\boldsymbol{\xi} + \frac{\alpha}{2}\boldsymbol{\omega}) + b(\boldsymbol{\xi})]\, d\boldsymbol{\xi} = \mathbf{0}$, we obtain that for the families (21) we have that $D\boldsymbol{\varphi}(\mathbf{0}) = \mathbf{0}$, which is an even more severe degeneracy than that of a typical (25).

The application of KAM theory to one dimensional parameter foliation preserving families of maps, which may be degenerate as above (but which satisfy other weaker non-degeneracy conditions), is developed in [20]. This reference also contains estimates on the measure of the parameters for which KAM theorem applies. In what follows, we will summarize the results of this paper to be able to apply it in Sec. V E to the problem of the cavity.

We recall that a family $\mathbf{f}^{\lambda}$ of mappings is said to be a C^r family when $\mathbf{f}^{\lambda}(\boldsymbol{\xi})$ is a C^r function of both $\boldsymbol{\xi}$ and λ (i.e., that it has continuous mixed derivatives of order up to r with respect to either $\boldsymbol{\xi}$ or λ).

Theorem III.2 *Let $\boldsymbol{\omega}_0 \in \mathbb{R}^d$ be an affine Diophantine vector of exponent ν. Let $\mathbf{f}^\lambda$ be a one-parameter C^r family of foliation-preserving mappings as in* (25) *such that $\mathbf{f}^0 = \mathbf{t}_{\boldsymbol{\omega}_0}$.*

Assume that the function $\tilde{\varphi}$ defined by $\tilde{\varphi}(\lambda)\boldsymbol{\omega}_0 = \int_{\mathbb{T}^d}[\mathbf{f}^\lambda(\boldsymbol{\xi}) - \boldsymbol{\xi}]\, d\boldsymbol{\xi}$ satisfies

$$\frac{d^N}{d\lambda^N}\tilde{\varphi}(\lambda)|_{\lambda=0} \neq 0$$

for some positive $N < r$. Assume also that r is large enough depending on the Diophantine exponent of $\boldsymbol{\omega}_0$.

Then, there is a set $\mathcal{B} \subset [-1, 1]$ such that:

a) For $\lambda \in \mathcal{B}$, $\mathbf{f}^\lambda$ is conjugate to the translation $\mathbf{t}_{u(\lambda)\boldsymbol{\omega}_0}$, i.e., there exists a diffeomorphism $\mathbf{h}^\lambda$ of the torus such that

$$\mathbf{f}^\lambda = (\mathbf{h}^\lambda)^{-1} \circ \mathbf{t}_{u(\lambda)\boldsymbol{\omega}_0} \circ \mathbf{h}^\lambda \ . \tag{38}$$

b) For some $C > 0$, and for all sufficiently small $\delta > 0$

$$|[-\delta, \delta] \cap \mathcal{B}^c| \leq C\delta^{1/N} \ ,$$

where $|\ \ |$ denotes the Lebesgue measure, and $\mathcal{B}^c$ is the complement of $\mathcal{B}$.

In typical situations, the set $\mathcal{B}$ is a Cantor set (i.e., it is a totally disconnected closed set). Note also that the maps $\mathbf{f}^\lambda$ satisfying the conclusions of KAM theorem (38) have a rotation number $u(\lambda)\boldsymbol{\omega}_0$.

Remark III.11 *Note also that a corresponding result for higher-dimensional parameters can be obtained from the one-dimensional case by decomposing the several-parameter family into several one-parameter families and repeatedly applying the one dimensional result.*

Remark III.12 *The results of [20] also include that the maps $\lambda \mapsto \mathbf{h}^\lambda$ and $\lambda \mapsto u(\lambda)$ can be extended to C^s functions on $[0, 1]$ where s is a number that depends on r and the Diophantine exponent ν. (Of course, the extended family will only satisfy Eq.* (38) *when $\lambda \in \mathcal{B}$.) This is sometimes referred to as saying that the function $\mathbf{h}^\lambda$ is* differentiable in the sense of Whitney *since [59] gave an intrinsic characterization of functions defined in closed sets that can be extended to smooth functions.*

Remark III.13 *When Theorem III.2 applies we expect that the rotation number changes when we change the parameters by arbitrarily small amounts. Similar results for circle maps are proved in [49].*

One of the consequences of the theory developed in [20] is that it is possible to derive formulas for the change of the rotation vector in the KAM region.

More explicitly, in [20] it is shown that, given $\mathbf{f}^{\boldsymbol{\lambda}}$*, a smooth enough family of diffeomorphisms of the torus indexed by an* ℓ*-dimensional parameter* $\boldsymbol{\lambda}$*, if* $\mathbf{f}^{\boldsymbol{\lambda}_0} = \mathbf{h}^{-1} \circ T_{u\boldsymbol{\omega}} \circ \mathbf{h}$ *and* $\mathbf{h}$ *is differentiable enough, then when* $\boldsymbol{\lambda} \approx \boldsymbol{\lambda}_0$ *and* $\boldsymbol{\lambda}$, $\boldsymbol{\lambda}_0$ *are such that the KAM theorem applies, the rotation vector of* $\mathbf{f}^{\boldsymbol{\lambda}}$ *is given by*

$$\boldsymbol{\rho}(\mathbf{f}^{\boldsymbol{\lambda}}) = \boldsymbol{\rho}(\mathbf{f}_0^{\boldsymbol{\lambda}}) + \left[\int_{\mathbb{T}^d} D\mathbf{h} \circ f \circ \mathbf{h}^{-1}(x) \frac{\partial}{\partial \lambda} \mathbf{f}^{\boldsymbol{\lambda}_0} \circ \mathbf{h}^{-1}(x)\, dx\right] (\boldsymbol{\lambda} - \boldsymbol{\lambda}_0) + O(|\boldsymbol{\lambda} - \boldsymbol{\lambda}_0|^2) \ . \quad (39)$$

The expression in the right-hand side of (39) *can be easily guessed by perturbation theory. The mathematical justification uses KAM techniques.*

Note that in the maps of the form (25),

$$\frac{\partial}{\partial \lambda} \mathbf{f}^{\boldsymbol{\lambda}_0} \circ \mathbf{h}^{-1}(x) = \boldsymbol{\omega} \frac{\partial}{\partial \lambda} \Gamma^{\boldsymbol{\lambda}_0} \circ \mathbf{h}^{-1}(x) \ .$$

It is clear that then the derivative of the rotation with respect to parameters is not zero in the KAM region for generic maps, for generic maps of the form (25) *and for generic maps appearing in the cavity problem.*

Numerical explorations in Sec. IV indicate that in the intervals of the complement of $\mathcal{B}$ (i.e., in the gaps of $\mathcal{B}$) one often has dynamics with negative Lyapunov exponent.

G. Structure of Dg, Lyapunov exponents, and hyperbolicity

An important measure of instability of a map $\mathbf{f}$ is the *Lyapunov exponent* defined by

$$\mu(\boldsymbol{\xi}, \mathbf{v}) \equiv \lim_{n\to\infty} \frac{1}{n} \log \|D\mathbf{f}^n(\boldsymbol{\xi})\, \mathbf{v}\| \ . \quad (40)$$

We recall that, by Oseledets theorem [60–62], the limits in (40) exist for all $\mathbf{v}$ and m-almost all $\boldsymbol{\xi}$ for any $\mathbf{f}$-invariant Borel measure m. It is clear that for every $\boldsymbol{\xi}$, there are at most d possible values of the limit in (40).

Lyapunov exponents are a rather weak notion of exponential growth of perturbations (or decay if they are negative). In particular, they ignore polynomial growth, and can be reached non-uniformly, i.e., at different rate for different points $\boldsymbol{\xi}$.

These general notions can be made more explicit for maps of the form (25). Notably, all but one of their Lyapunov exponents are zero.

Proposition III.1 *Let* $\mathbf{g}$ *be a* $C^1 : \mathbb{T}^d \to \mathbb{T}^d$ *map of the form* (25). *Then for every point* $\boldsymbol{\xi} \in \mathbb{T}^d$, $d-1$ *of the Lyapunov exponents of* $\mathbf{g}$ *are 0. Beside these* $d-1$ *trivial exponents, for* m*-almost every* $\boldsymbol{\xi}$ *there is one Lyapunov exponent corresponding to the direction of* $\boldsymbol{\omega}$*.*

Proof. For foliation preserving maps $\mathbf{g}$,

$$D\mathbf{g}(\boldsymbol{\xi})\,\boldsymbol{\omega} = [1 + \boldsymbol{\omega}\cdot\nabla\Gamma(\boldsymbol{\xi})]\,\boldsymbol{\omega} := \lambda(\boldsymbol{\xi})\,\boldsymbol{\omega}\ . \tag{41}$$

Let us choose a system of (affine) coordinate patches of $\mathbb{T}^d$ in the following way: Choose an orthonormal frame $\mathbf{v}_1, \ldots, \mathbf{v}_d$ in $\mathbb{R}^d$ in such a way that $\mathbf{v}_1 = \boldsymbol{\omega}$. Let U be the orthogonal matrix that transforms the standard basis of $\mathbb{R}^d$ into $\mathbf{v}_1, \ldots, \mathbf{v}_d$. Define the charts $\boldsymbol{\psi}_i : B_{1/10} \to \mathbb{T}^d$ (where $B_{1/10}$ is the ball of radius $\frac{1}{10}$ around the origin in $\mathbb{R}^d$) by

$$\boldsymbol{\psi}_i(\mathbf{x}) = \mathbf{\Pi}(U\mathbf{x} + \mathbf{t}_i)\ , \tag{42}$$

where $\mathbf{\Pi}$ is given by (19), and $\{\mathbf{t}_i\}$ is a finite set of translations in a grid of size, say, $\frac{1}{100}$, to ensure that the union $\cup_i \boldsymbol{\psi}_i(B_{1/10})$ cover the whole $\mathbb{T}^d$. Then in all coordinate patches, the differential $D\mathbf{g}(\boldsymbol{\xi})$ has the form

$$D\mathbf{g}(\boldsymbol{\xi}) = U^{-1}\begin{pmatrix} \lambda(\boldsymbol{\xi}) & * & * & \cdots & * \\ 0 & 1 & 0 & \cdots & 0 \\ 0 & 0 & 1 & \cdots & 0 \\ \vdots & \vdots & \vdots & \ddots & \vdots \\ 0 & 0 & 0 & \cdots & 1 \end{pmatrix} U\ , \tag{43}$$

where the stars represent numbers that are nonzero in general. Hence, the differential of the iterated map, $D\mathbf{g}^n(\boldsymbol{\xi})$, after conjugating with U, is also upper triangular with the first element in the diagonal equal to $\lambda(\mathbf{g}^{n-1}(\boldsymbol{\xi}))\cdots\lambda(\boldsymbol{\xi})$, and all other diagonal terms equal to 1. This makes it clear that $d-1$ Lyapunov numbers are equal to 0.

According to Birkhoff ergodic theorem,

$$\frac{1}{n}\log\left[\lambda(\mathbf{g}^{n-1}(\boldsymbol{\xi}))\cdots\lambda(\boldsymbol{\xi})\right] = \frac{1}{n}\left[\log\lambda(\mathbf{g}^{n-1}(\boldsymbol{\xi})) + \cdots + \log\lambda(\boldsymbol{\xi})\right]$$

has a limit as $n \to \infty$ for m-almost every $\boldsymbol{\xi}$, for any $\mathbf{g}$-invariant probability measure m. This limit is, of course, another Lyapunov exponent besides the previously found $d-1$

equaling zero. (It could, of course, happen that this exponent is zero.) □

Remark III.14 *Note that in this case, since we are considering the Lyapunov exponent along one dimensional bundles, we can establish the existence of the Lyapunov exponent using the Birkhoff ergodic theorem rather that the more elaborate Osledec ergodic theorem customary in the theory of Lyapunov exponents.*

We also note that in the cases that will be of most interest to us (KAM and attracting invariant circles, there will be only one invariant measure. Hence, in those cases, we can speak about the Lyapunov exponent without specifying the invariant measure.

In particular, the differential $D\mathbf{g}$ of the torus map $\mathbf{g}$ (21) is

$$D\mathbf{g}(\boldsymbol{\xi}) = \left[\mathrm{Id} - \boldsymbol{\omega} \otimes \nabla\Phi(\mathbf{g}(\boldsymbol{\xi}))\right]^{-1}\left[\mathrm{Id} + \boldsymbol{\omega} \otimes \nabla\Phi(\boldsymbol{\xi})\right] . \tag{44}$$

Therefore,

$$D\mathbf{g}(\boldsymbol{\xi})\, \boldsymbol{\omega} = \lambda(\boldsymbol{\xi})\boldsymbol{\omega} ,$$

where

$$\lambda(\boldsymbol{\xi}) \equiv \frac{1 + \boldsymbol{\omega} \cdot \nabla\Phi(\boldsymbol{\xi})}{1 - \boldsymbol{\omega} \cdot \nabla\Phi(\mathbf{g}(\boldsymbol{\xi}))} . \tag{45}$$

Hence,

$$D\mathbf{g}^n(\boldsymbol{\xi})\, \boldsymbol{\omega} = \lambda(\mathbf{g}^{n-1}(\boldsymbol{\xi})) \cdots \lambda(\boldsymbol{\xi})\, \boldsymbol{\omega} ,$$

so the Lyapunov exponent in the direction of $\boldsymbol{\omega}$ is equal to the average of the logarithm of λ along the orbit of $\boldsymbol{\xi}$, and the other $d-1$ Lyapunov exponents are equal to 0.

One important notion in the theory of Lyapunov exponents is the *Lyapunov splitting*, in which we associate a space $E^i_{\boldsymbol{\xi}}$ to each base point $\boldsymbol{\xi}$ and each Lyapunov exponent λ_i.

Even if the previous argument identifies $\boldsymbol{\omega}$ as the space corresponding to the possibly non-trivial exponent, the space corresponding to all the Lyapunov exponents zero is not so easy to identify. Even in the uniformly hyperbolic case (see below), the dependence of $E^i_{\boldsymbol{\xi}}$ on $\boldsymbol{\xi}$ can be a non-smooth function.

A notion which in principle is stronger than the existence of a positive Lyapunov exponent is that of uniform hyperbolicity. In our case, since we only have one direction with non-trivial expansion, this notion reduces to the following:

Definition III.5 *We say that a set $\mathcal{L} \subset \mathbb{T}^d$ invariant by* $\mathbf{f}$ *as in* (21) *is* uniformly attracting, *(resp. expanding) when there exist constants $C > 0$, $\alpha > 0$, such that we can find a splitting $T_{\boldsymbol{\xi}}\mathbb{T}^d = (\operatorname{span}\boldsymbol{\omega}) \oplus E^s_{\boldsymbol{\xi}}$ (resp. $T_{\boldsymbol{\xi}}\mathbb{T}^d = (\operatorname{span}\boldsymbol{\omega}) \oplus E^u_{\boldsymbol{\xi}}$) such that*

$$\|D\mathbf{f}^n(\boldsymbol{\xi})\,\mathbf{v}\| \;\le\; Ce^{-\alpha n}\|\mathbf{v}\| \;, \quad \forall n \in \mathbb{N} \;, \quad \boldsymbol{\xi} \in \mathcal{L} \;, \quad \mathbf{v} \in E^s_{\boldsymbol{\xi}}$$
$$(\text{ resp. } \|D\mathbf{f}^n(\boldsymbol{\xi})\,\mathbf{v}\| \;\ge\; Ce^{\alpha n}\|\mathbf{v}\| \;, \quad \forall n \in \mathbb{N} \;, \quad \boldsymbol{\xi} \in \mathcal{L} \;, \quad \mathbf{v} \in E^s_{\boldsymbol{\xi}} \;) \;.$$

Uniformly attracting or uniformly repelling sets have some remarkable properties. For example, the general theory of persistence of normally hyperbolic sets [63–65] implies, for our case, the following theorem.

Theorem III.3 *Let* $\mathbf{g}$ *be a map of the form* (25).

Assume that there exists a compact set $\mathcal{L} \subset \mathbb{T}^d$ invariant under $\mathbf{g}$ *such that*

(i) $\mathcal{L}$ is a C^1 manifold without boundary;

(ii) $\mathcal{L}$ is transversal to $\operatorname{span}\boldsymbol{\omega}$ *at each point: $T_{\boldsymbol{\xi}}\mathcal{L} \oplus \operatorname{span}\boldsymbol{\omega} = \mathbb{R}^d$;*

(iii) $\mathbf{g}|_{\mathcal{L}}$ is uniformly attracting (resp. repelling).

Then,

(a) For any torus map $\mathbf{g}'$ sufficiently C^1-close to $\mathbf{g}$, we can find a set $\mathcal{L}'$ invariant under $\mathbf{g}'$ and satisfying (i), (ii) and (iii).

(b) If $\mathbf{g}$ is sufficiently differentiable, we can conclude that $\mathcal{L}$ is C^r where r is a finite number determined by the ratios of the logarithms of the normal contraction rates and the logarithms of the Lipschitz constant of the restriction $\mathbf{g}|_{\mathcal{L}}$ and its inverse.

Notice that (ii) and (iii) are a formulation of normal hyperbolicity in the sense of [63–65]. Also, note that since $T\mathcal{L}$ is invariant, it has to be identified with the space corresponding to the zero Lyapunov exponent.

It is important to note that the general theory of normal hyperbolicity does not allow us to conclude that invariant manifolds are C^∞ – much less analytic – even if the torus map is analytic. Nevertheless, in the case that $d = 2$, using the fact that the map is of the form (25), it is possible to show that they are analytic (see Lemma III.3).

We will argue later that the existence of manifolds satisfying the hypothesis of Theorem III.3 is an analogue for maps of the form (25) of the phase locking that happens frequently in circle maps.

Theorem III.3 is interesting from our point of view because its hypotheses are verified on open sets of parameters (we will argue that these sets are non-empty and give more precise information about their shape). We will also show that their existence has important consequences for the behavior of the electromagnetic field in the cavity.

Note that in the case $d = 2$ and the manifold $\mathcal{L}$ is a one dimensional torus, the map restricted to $\mathcal{L}$ has a rotation number. This case will be considered in greater detail in the numerical experiments. As mentioned before, this case allows us to conclude more regularity.

H. Resonances

Resonances are a generalization of the phase locking encountered in circle maps with rational rotation numbers, when the circle map has an attracting or repelling periodic point. Recall that the origin of the phase locking is that, by the implicit function theorem, these periodic points persist, hence the rotation number remains constant for small enough perturbations of the map. For higher dimensional tori, there are situations, which we will argue are very similar, namely, when there is an invariant circle (or a set of circles permuted by the map) satisfying the hypothesis of Theorem III.3. The circles are analogues of the periodic fixed points and Theorem III.3, guaranteeing the persistence of these objects, plays the same role as the implicit function theorem does for periodic points.

A situation that will appear in practice very often is that we have a finite collection of manifolds $\mathcal{L}_1, \ldots, \mathcal{L}_n$ in such a way that $\mathbf{g}(\mathcal{L}_i) = \mathcal{L}_{i+1}$ for $i = 1, \cdots, n-1$ $\mathbf{g}(\mathcal{L}_{n-1}) = \mathcal{L}_1$. We will refer to this situation as saying that there is an invariant orbit of manifolds (often they will be circles). Clearly, each of the $\mathcal{L}_i$ is an invariant manifold for $\mathbf{g}^n$. Hence, many of the results for invariant circles apply to this, slightly more general situation. To simplify the notation, we will often discuss only invariant circles when it is clear that the results apply also to invariant orbits of manifolds.

1. *Rotation vectors and invariant circles*

Our first task is to elucidate the consequences of the existence of these invariant objects to the rotation set.

Definition III.6 *We say that a rotation vector* $\boldsymbol{\omega}$ *is* $(\mathbf{k}, n)$-resonant *(for* $\mathbf{k} \in \mathbb{Z}^d \setminus \{\mathbf{0}\}$*,* $n \in \mathbb{Z}$*) if*

$$\mathbf{k} \cdot \boldsymbol{\omega} = n \ .$$

Note that the set of $\mathbf{k}$'s for which a vector is resonant is a $\mathbb{Z}$-module.

Note also that the set of $(\mathbf{k}, n)$-resonant vectors is a hyperplane of codimension one in the space of frequencies with normal direction $\mathbf{k}$. Hence, given a vector $\boldsymbol{\omega}_0$ that is incommensurate (and, therefore, not perpendicular to any $\mathbf{k} \in \mathbb{Z}^d \setminus \{\mathbf{0}\}$), we can find $t \in \mathbb{R}$ such that $t\boldsymbol{\omega}_0$ is $(\mathbf{k}, n)$-resonant.

A translation $\mathbf{t}_{\boldsymbol{\rho}}$ where $\boldsymbol{\rho}$ is resonant preserves a family of invariant tori. If we make a more or less arbitrary perturbation, most of the invariant tori disappear, but there is a discrete set of tori that survive the perturbation and satisfy the hypothesis of Theorem III.3 (for precise statements about the non-degeneracy conditions, regularity, etc. that are required on the perturbation, we refer to [21, 66].) This is quite analogous of the situation in maps of the circle when a perturbation of a rational rotation leads the existence of attractive and repulsive periodic orbits.

Hence, in the perturbative case, there is a relation between resonant rotation number and the existence of tori satisfying the hypothesis of Theorem III.3.

Some other relations can be found in the non-perturbative regime. We will only discuss the case $d = 2$ in which the attractive and repelling invariant tori of codimension 1 are circles.

Since this will appear repeatedly in our arguments, we introduce the notation that a circle is of type $\mathbf{k}$, when it is homotopic to the set $\{\boldsymbol{\xi} \in \mathbb{T}^2 | \ \boldsymbol{\xi} \cdot \mathbf{k} = 0\}$. To avoid ambiguities, we assume that $\mathbf{k} \in \mathbb{Z}^2 \setminus \{\mathbf{0}\}$ has components that are relatively prime. We write this circle as the image of the map $t \mapsto t\mathbf{k}^\perp$, $t \in \mathbb{T}^1$.

For us, the following converse is important

Lemma III.1 *Assume that the diffeomorphism* $\mathbf{g} : \mathbb{T}^2 \to \mathbb{T}^2$ *has a topological invariant circle* $\mathcal{L}$ *of type* $\mathbf{k}$*, and let* $\mathbf{g}|_{\mathcal{L}}$ *have rotation number* γ*.*

Then the rotation set of the diffeomorphism f contains $\mathbf{k}^{\perp}\gamma$.

Note that if the invariant circles appearing in the hypothesis of Lemma III.1 are attracting or repelling, by Theorem III.3, the circles are differentiable, and they persist for small perturbations. Hence, for all perturbations we can ensure that the rotation set contains points of the form $\mathbf{k}^{\perp}\gamma$ where γ is the rotation number of the perturbed invariant circle.

2. Some rigidity properties of attracting invariant circles

Naively, one might think that it is possible to make perturbations that change the rotation number of these attractive circles. However it turns out that

Lemma III.2 *Let $\mathbf{f}, \mathbf{g} : \mathbb{T}^2 \to \mathbb{T}^2$ be C^1 maps of the form (25) with $\Gamma_{\mathbf{f}}, \Gamma_{\mathbf{g}} \geq \delta > 0$. Assume that $\mathbf{f}$ and $\mathbf{g}$ are sufficiently C^1 close. Assume that $\mathbf{f}$ has a uniformly attracting invariant circle $\mathcal{L}_{\mathbf{f}}$. Denote by $\mathcal{L}_{\mathbf{g}}$ the invariant circle obtained by applying Theorem III.3 to $\mathbf{g}$.*

Then, $\mathbf{f}|_{\mathcal{L}_{\mathbf{f}}}$ has the same rotation number as $\mathbf{f}|_{\mathcal{L}_{\mathbf{g}}}$. This number is irrational.

The proof of this Lemma is very simple. We know that if the rotation number of $\mathbf{f}|_{\mathcal{L}_{\mathbf{f}}}$ was rational, then $\mathbf{f}$ should have a periodic point, which is impossible for maps of the form (25) with $\Gamma > 0$.

Since $\mathbf{g}|_{\mathcal{L}_{\mathbf{g}}}$ depends continuously on $\mathbf{g}$, if the rotation number changed, then, at some intermediate point it would have to take rational values, which is not allowed.

Indeed, two maps $\mathbf{f}|_{\mathcal{L}_{\mathbf{f}}}$, $\mathbf{g}|_{\mathcal{L}_{\mathbf{g}}}$ are differentiably conjugate. The conjugacy is given by the holonomy map of the foliation.

Note that, if $\mathbf{h}(\boldsymbol{\xi})$ is the holonomy map of a point $\boldsymbol{\xi}$ from $\mathcal{L}_{\mathbf{f}}$ to $\mathcal{L}_{\mathbf{g}}$, then $\mathbf{f}(\boldsymbol{\xi})$ is in the same leaf of the foliation as $\boldsymbol{\xi}$, and $\mathbf{g} \circ \mathbf{h}(\boldsymbol{\xi})$ is in the same leaf as $\mathbf{h}(\boldsymbol{\xi})$. Hence, $\mathbf{g} \circ \mathbf{h}(\boldsymbol{\xi})$ is in the same leaf of the foliation as $\mathbf{f}(\boldsymbol{\xi})$. Therefore, $\mathbf{h} \circ \mathbf{f}(\boldsymbol{\xi}) = \mathbf{g} \circ \mathbf{h}(\boldsymbol{\xi})$, see Figure 3.

The preceding discussion makes it clear that the attracting (repelling) invariant circles of maps of the form (25) with $\Gamma > 0$ are extremely rigid.

At the moment, we do not have many rigorous results on this, but we will present some numerical explorations in Section IV.

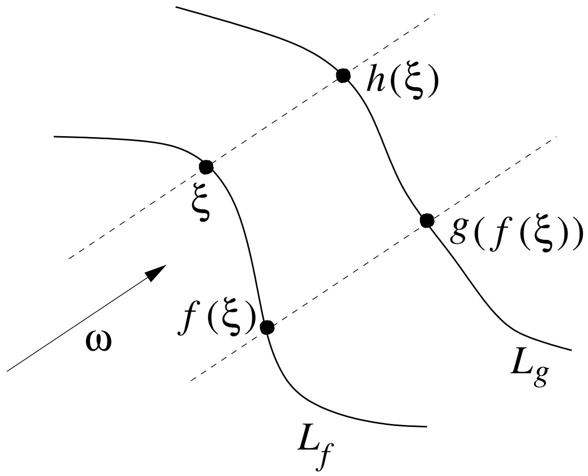

FIG. 3: Conjugacy $\mathbf{h}$ between $\mathbf{f}$ and $\mathbf{g}$.

3. *Analyticity of invariant circles and non-stationary normal forms*

We note that since these mappings preserve a foliation and their iterates are moving quasiperiodically, in an appropriate system of coordinates, they can be described as a skew product on the set $(x, \theta) \in (-1, 1) \times \mathbb{T}^1$:

$$x \mapsto f(x + \rho) \ , \quad \theta \mapsto \theta + \rho \ . \tag{46}$$

Some of the bifurcations of the invariant circles of skew products have been studied in [43]. Among the bifurcations understood rigorously, there are analogues of the classical period doubling and saddle node bifurcations. There is also a numerical evidence of others.

In our case, since the invariant circle eventually changes rotation number, there have to be significantly more complicated phenomena that break the skew product structure (46).

We remark also that, by Theorem III.3, when this situation happens, it is robust in the sense that it will also happen if we slightly modify the conditions of the problem (in particular, if we slightly modify the parameters α, β, γ of (5)).

The structure given by (46) and the fact that the rotation number is Diophantine (it has to be a rational linear combination of the components, which are Diophantine affine) allow us to refine the regularity conclusions of the general normal hyperbolicity theory summarized in Theorem III.3.

To set up the stage for these improvements, we start by making some easy observations. Assume that $\mathbf{g}$ is of the form (25), with $\boldsymbol{\omega}$ Diophantine affine and analytic. Note that if the vector $\boldsymbol{\omega}$ is Diophantine affine, the rotation number of the map restricted to $\mathcal{L}$ is

Diophantine. By applying Theorem III.1 to the motion restricted to $\mathcal{L}$ – recall that, by Theorem III.3 we have that $\mathcal{L}$ is differentiable – we can obtain that the motion on $\mathcal{L}$ is conjugate to a Diophantine rotation. In particular, by Weyl's theorem, it preserves only an invariant measure m (the push-forward by the conjugacy of the Lebesgue measure on the circle).

The fact that $\mathbf{g}|_{\mathcal{L}}$ preserves only one invariant measure shows that there is only one possibly non-zero Lyapunov exponent μ which can be obtained by taking $\mu = \int_{\mathcal{L}} \log(|D\mathbf{g}(x)\boldsymbol{\omega}|/|\boldsymbol{\omega}|)\, dm(x)$.

Lemma III.3 *Assume that* $\mathbf{g}$ *is a map of the form* (25)*, for a two dimensional torus. Assume that the direction of the vector* $\boldsymbol{\omega}$ *the preserved foliation is Diophantine affine. Let* $\mathcal{L}$ *be an invariant circle satisfying the hypothesis of Theorem III.3.*

Then:

(a) The circle $\mathcal{L}$ *is an analytic manifold.*

(b) There exists an analytic change of variables $\boldsymbol{\Psi}$ *defined in a neighborhood of* $\mathcal{L}$ *to* $(-1,1)\times\mathbb{T}^1$ *such that*

(b.1) $\boldsymbol{\Psi}(\mathcal{L}) = \{0\}\times\mathbb{T}^1$*;*

(b.2) $\boldsymbol{\Psi}\circ\mathbf{g}(x,\theta) = \boldsymbol{\Psi}(\mu x, \theta+\rho)$*.*

That is, in the appropriate coordinates given by $\boldsymbol{\Psi}$, the effect of $\mathbf{g}$ in a neighborhood of $\mathcal{L}$ is simply to contract by a constant factor the normal coordinate and to rotate the angle coordinate.

Note that the systems of coordinates given by Ψ provides with a sort of non-autonomous linearization of the motion of the map around $\mathcal{L}$. In this system of coordinates, the motion is exactly linear.

Similar systems of coordinates to those constructed in Lemma III.3 exist in the general theory of normally hyperbolic manifolds. Of course, in the general case these objects are only finitely differentiable and one cannot reduce the motion in the normal directions exactly to linear. These results have been considered in [64, 67, 68] and, with a different flavor, in [69].

We omit the details of the proof of Lemma III.3 and refer to [21].

We indicate that, in the coordinates given by (46), $\mathbf{g}$ is a fiber contraction in the adapted norm. This allows us to describe $\mathcal{L}$ as the graph of a function. The invariance of this graph is equivalent to the function satisfying a functional equation that can be solved by a contraction argument in a space of analytic functions. This allows us to make an analytic change of coordinates in such a way that $\mathbf{\Psi}(\mathcal{L}) = \{0\} \times \mathbb{T}^1$. Then, one can simply derive a functional equation for $\mathbf{\Psi}(y, \theta) - (y, 0)$ and show that this equation can be solved by a fixed point argument in a space of analytic functions.

The interpretation of Lemma III.3 and especially the interpretation of the normal form around the circle are given in Lemma V.1.

4. Pairs of attractive and repulsive periodic circles

A situation we encounter very often in a phase locked region is the following: There is an attracting invariant periodic orbit of circles $\mathcal{L}^+$ as well as a repulsive invariant periodic orbit of circles $\mathcal{L}^-$.

Moreover, all the points of $\mathbb{T}^2 \setminus \mathcal{L}^-$ (resp. $\mathbb{T}^2 \setminus \mathcal{L}^+$) are attracted under forward (resp. backward) iteration to $\mathcal{L}^+$ (resp. $\mathcal{L}^-$). For an illustration of this situation, see Figure 6. The boundary of the basin of attraction of $\mathcal{L}^+$ under forward iteration is precisely $\mathcal{L}^-$. Similarly, the boundary of the basin of attraction of $\mathcal{L}^-$ under backward iteration is $\mathcal{L}^+$.

This pairing of attracting and repelling circles is quite natural since it is a very easy topological argument that in the torus it is impossible to have attracting circles whose basin covers the whole circle.

By the argument depicted in Figure 3, it is clear that the motion of the iterates of $\mathbf{f}$ in $\mathcal{L}^+$ is conjugate to that in $\mathcal{L}^-$. Hence, $\mathbf{f}|_{\mathcal{L}^+}$ and $\mathbf{f}_{\mathcal{L}^-}$ have the same rotation number.

Since all points get attracted to $\mathcal{L}^+$ or lie on $\mathcal{L}^-$, it is not difficult to show that in this case the rotation set is just a point. Thus, the rotation vector exists in both of the extreme cases: the KAM case and the typical phase locking one.

We point out that the existence of situations as above can be established rigorously in perturbations of rigid translations. The paper [66] contains a perturbation analysis of rotations perturbed by trigonometric polynomials. In [21], this analysis is extended to more general perturbations, and also to the maps arising in the problem of the resonant cavity.

The perturbative analysis of the regions where these resonances exist can be made quite analogous to the study of Arnol'd tongues in the circle maps.

The analysis of [21] shows that given a two parameter family of maps $\mathbf{f}^{\boldsymbol{\lambda}}$, where λ_1 is a parameter controlling the rotation and λ_2 is a parameter controlling the non-linearity, the regions where the resonance occur will be tongues described as $|\lambda_2 - a| \le |\lambda_1 - b|^\eta C + O(|\lambda_1 - b|^{\eta'})$ where $\eta < \eta'$ are rational numbers. The numbers η, η', C can be computed rather explicitly out of the Fourier expansion of the perturbed map.

One of the conclusions of the analysis is that the asymptotic width of the tongues created by resonances is different for the maps arising in the cavity problem and for the typical maps of the form (25). In particular, for maps appearing in the cavity, we always have $\eta > 1$. This is in contrast with the behavior of a generic map of the torus which has tongues with $\eta = 1$. (For an analysis of circle maps see [70, 71].) For a numerical illustration see Figure 14. The consequences of this dynamic behavior for the oscillating cavity are discussed in Section V D.

IV. NUMERICAL STUDY OF THE CAVITY TORUS MAPS

In this section we report the results of our numerical investigation of the map $\mathbf{g} : \mathbb{T}^2 \to \mathbb{T}^2$ corresponding to the motion of the boundary of the cavity given by (1), (5), (6). Unless otherwise specified, in the whole section $\mathbf{g}$ will stand for this particular map.

A. General remarks

As we noted in Sec. III E, the rotation set of $\mathbf{g}$ must be an interval proportional to the frequency vector $\boldsymbol{\omega}$ which for motion of the mirror given by (5), (6) is $\boldsymbol{\omega} = (1, \sigma_{\mathrm{G}})$. Based on our numerical investigations, we adopt the working hypothesis that the rotation set for the torus maps in our problem consists only of one element which we call a rotation vector. We have not found any evidence to the contrary. This assumption is true, i.e. it is proven, for the situations (phase locking and KAM regions) which will be the main focus of our investigations.

For the map (5), (6), the rotation vector $\boldsymbol{\tau}(\mathbf{g})$ has only one independent component, because it has to be a multiple of $\boldsymbol{\omega}$:

$$\boldsymbol{\tau}(\mathbf{g}) = \rho\boldsymbol{\omega} = \rho\,(1, \sigma_{\mathrm{G}}) \ . \tag{47}$$

For reasons that will become clear in Sec. IV A, we will call the first component, $\tau_1(\mathbf{g}) = \rho\omega_1 = \rho$, of $\boldsymbol{\tau}(\mathbf{g})$ a *rotation number* of the map $\mathbf{g}$. Note that because of the incommensurability of $\boldsymbol{\omega}$ and condition (3), the map $\mathbf{g}$ has no periodic points.

Due to the existence of an invariant foliation $\mathcal{F}_{\boldsymbol{\omega}}$, for any dimension d of the torus, the problem we have to solve numerically is still essentially one-dimensional. Indeed, let θ_n be the time of the n^{th} reflection of a particular ray from the moving mirror, and $\boldsymbol{\xi}_n = \mathbf{\Pi}(\boldsymbol{\omega}\theta_n)$ be the vector of the phases of the mirror's motion at that moment. To find $\boldsymbol{\xi}_{n+1} = \mathbf{g}(\boldsymbol{\xi}_n)$, we first find the time θ_{n+1} of the $(n+1)^{\text{st}}$ reflection of this ray from the moving mirror by solving numerically the relation (20). To compute θ_{n+1}, we used the zero finding routine ZBRENT from [72] (using `long double` precision). Having found θ_{n+1}, we compute $\boldsymbol{\xi}_{n+1} = \mathbf{g}(\boldsymbol{\xi}_n)$ from

$$\boldsymbol{\xi}_{n+1} = \mathbf{\Pi}\left(\boldsymbol{\xi}_n + (\theta_{n+1} - \theta_n)\boldsymbol{\omega}\right) \ .$$

To hone our intuition and to make a connection with the case $d = 1$, let us start with the case of the map (5) with $\gamma = 0$. As we will discuss later, the more complicated cases can be reduced to this one. In the case that $\gamma = 0$, the phase ξ_2 has no effect on the motion of the mirror. Therefore, the dynamics of the map $\mathbf{g}$ can be derived completely from the dynamics of the projection of $\mathbf{g}$ on the ξ_1 axis. If $\pi_1 : \mathbb{T}^2 \to \mathbb{T}^1 : (\xi_1, \xi_2) \mapsto \xi_1$ is the projection onto the ξ_1 axis, then the map $\tilde{g}$ defined by

$$\pi_1 \circ \mathbf{g} = \tilde{g} \circ \pi_1$$

is a circle map.

As an example, let us consider the map $\tilde{g}$ for $\beta = 0.1$, $\gamma = 0$, in which case the phase locking interval of values of α for which $\tilde{g}$ is phase locked with rotation number $\frac{1}{5}$ is

$$[0.273630763679\,,\, 0.275033857936] \ .$$

In Figure 4 we show 10000 iterates of $\mathbf{g}$ for $\alpha = 0.273631$, $\beta = 0.1$, $\gamma = 0$; the initial point is circled. Since for these values of the parameters, the map $\mathbf{g}$ is $(5, 0, 1)$-resonant, the iterates accumulate on an attractor consisting of five "vertical" lines.

The case in which the map $\tilde{g}$ is phase locked is of particular interest for us, because the case of a small "incommensurate perturbation" (which for the case of the phase advance map $\mathbf{g}$ corresponds to small values of γ in (5)) can be considered as a small perturbation to the map $\mathbf{g}$ with $\gamma = 0$. The theory of normally hyperbolic systems guarantees that if γ is

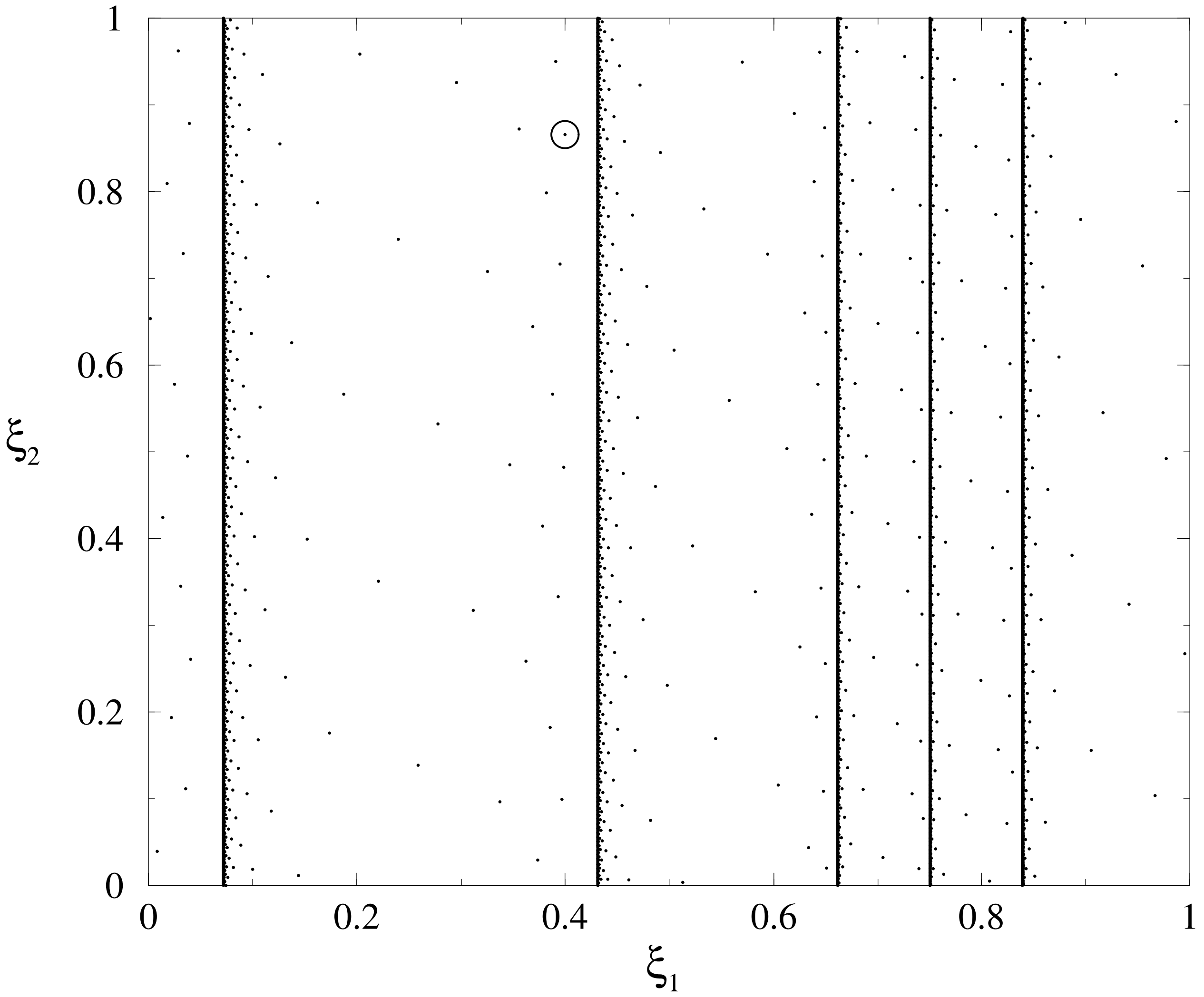

FIG. 4: Iterates of $\mathbf{g}$ in the case of $\tau = 1/5$ phase locking with $\gamma = 0$ (i.e., $(5, 0, 1)$-resonance).

small enough, the map $\mathbf{g}$ will remain $(q, 0, p)$-resonant. Examples of this phenomenon will be shown in Section IV B.

Remark IV.1 *The more general case of phase locking can be reduced by a change of variables to this one when we are near a pure rotation (or in a neighborhood of the invariant circle).*

In the perturbative case, the main idea is that near a frequency ω such that $\omega \cdot k = m$ and there are no other relations, given a map $\boldsymbol{\xi} \to \boldsymbol{\xi} + \omega + \epsilon\Gamma(\boldsymbol{\xi})$ it is possible to make a (linear) change of variables so that, in the new variables $\tilde{\boldsymbol{\xi}}$, the map is is expressed as

$$\tilde{\boldsymbol{\xi}} \to \tilde{\boldsymbol{\xi}} + \epsilon\tilde{\Gamma}(\boldsymbol{\xi} \cdot \mathbf{k}) + O(\epsilon^2). \tag{48}$$

Ignoring the $O(\epsilon^2)$ terms, the map (48) *is a circle map (along the component* $\boldsymbol{\xi} \cdot \mathbf{k}$*) and the identity along all the other components.*

For more details we refer to [21].

B. Exploration of parameter space

As a first diagnostic of the resonant regions, we have computed the Lyapunov exponent for randomly chosen orbits of $\mathbf{g}$ as a function of α and γ for fixed β. Up to the precision of the numerical computation, one expects that there is a resonance precisely at the places where the Lyapunov exponent of this orbit is negative.

A typical result is depicted in Figure 5, where we present the values of (α, γ) for which the map with $\beta = 0.13$ has Lyapunov exponent smaller than -0.03. For some parameter values inside the resonant regions (indicated with a cross in the figure), we have identified the type of the resonance by performing a direct iteration of the map.

The resonances of type $(3, 0, 2)$ and $(4, 0, 3)$ come from the $\frac{2}{3}$ and $\frac{3}{4}$ phase lockings of the map $\mathbf{g}$ with $\beta = 0.13$ and $\gamma = 0$, while the other resonances shown in the figure appear because of the incommensurate forcing.

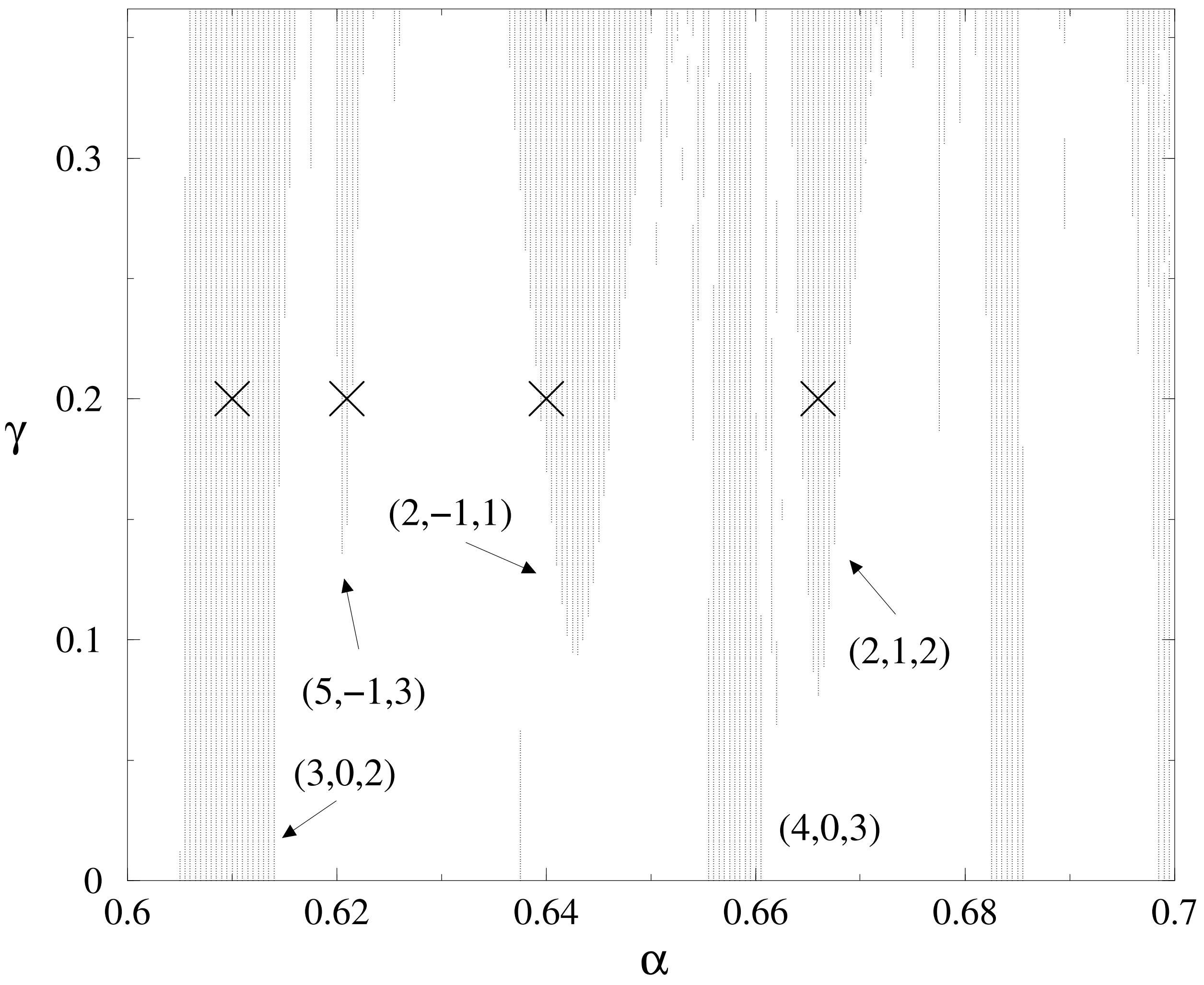

FIG. 5: Sketch of the resonant regions in the (α, γ) plane for $\beta = 0.13$.

In Figure 6, we depict the attracting (thick lines) and repelling (thin lines) invariant 1-dimensional tori of the map $\mathbf{g}$ for parameter values in the regions with negative Lyapunov exponent for which $\mathbf{g}$ is $(3, 0, 2)$-, $(5, -1, 3)$-, $(2, -1, 1)$-, and $(2, 1, 2)$-resonant, respectively.

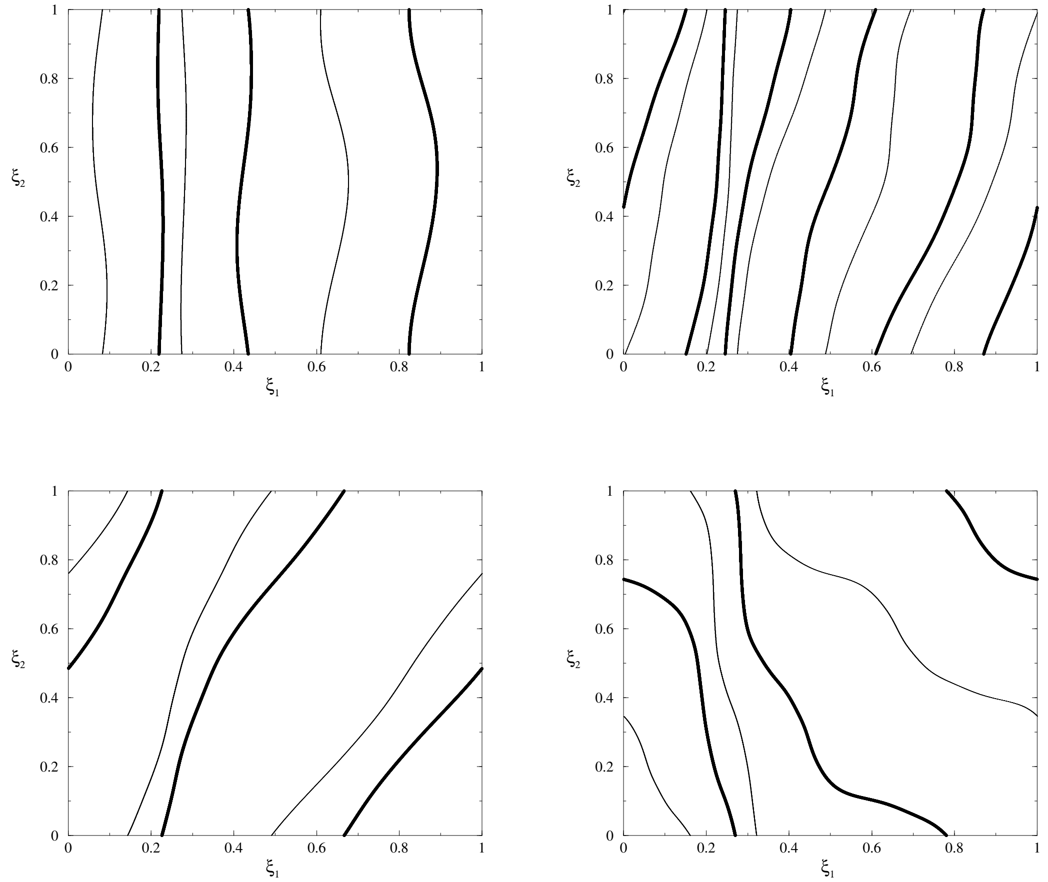

FIG. 6: Attracting and repelling circles for $\mathbf{g}$ in $(3,0,2)$-, $(5,-1,3)$-, $(2,-1,1)$-, and $(2,1,2)$-resonant cases.

In Figure 7, we give more detailed information about the Lyapunov exponents of the map $\mathbf{g}$ for $\beta = 0.13$ for the same range of α and γ as in Figure 5. The blue color corresponds to Lyapunov exponents with the smallest absolute value, the green one to the intermediate values, and the red one to the largest values.

To give a better idea about how rich the behavior near the boundary of the resonant zones is, we show in Figure 8 iterates of the map $\mathbf{g}$ for the same values of β and γ ($\beta = 0.13$, $\gamma = 0.2$) and different values of α. The values of α are very close to the value of α for the $(2,-1,1)$-resonant map from Figure 6. The values of α and the type of resonance are shown in the table; for $\alpha = 0.6389$, the map is $(2,-1,1)$-resonant as in the lower left corner of Figure 6.

The fact that the topological type of the attractive tori changes drastically for very small modifications of the parameter, we believe lends support to the idea that at the boundary

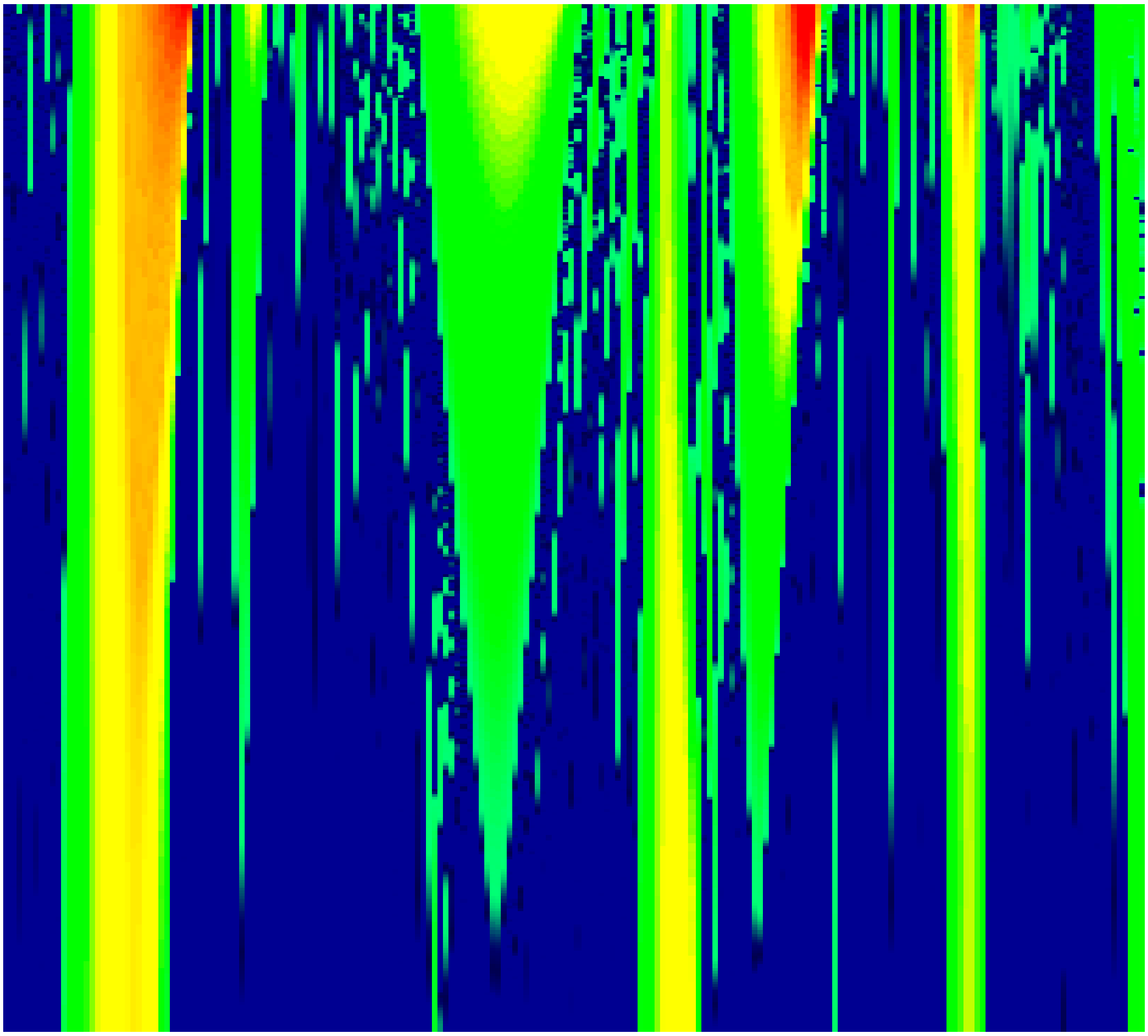

FIG. 7: Lyapunov exponents of the map $\mathbf{g}$ for $\beta = 0.13$ in the (α, γ)-plane for $\alpha \in [0.6, 0.7]$ (on the horizontal axis), and $\gamma \in [0, 0.362]$ (on the vertical axis).

of the resonance regions, the bifurcations are rather complicated and deserve further study.

Figure	α	ρ	**Resonance type**
8 (upper left)	0.6387	0.72192451 . . .	$(53, -23, 28)$
8 (upper right)	0.6386	0.72125379 . . .	$(37, -15, 20)$
8 (lower left)	0.6385	0.72074231 . . .	Non-resonant
8 (lower right)	0.6384	0.72025004 . . .	$(25, -9, 14)$

Even resonances with small m_1, m_2, and k, can occur for very close values of the param-

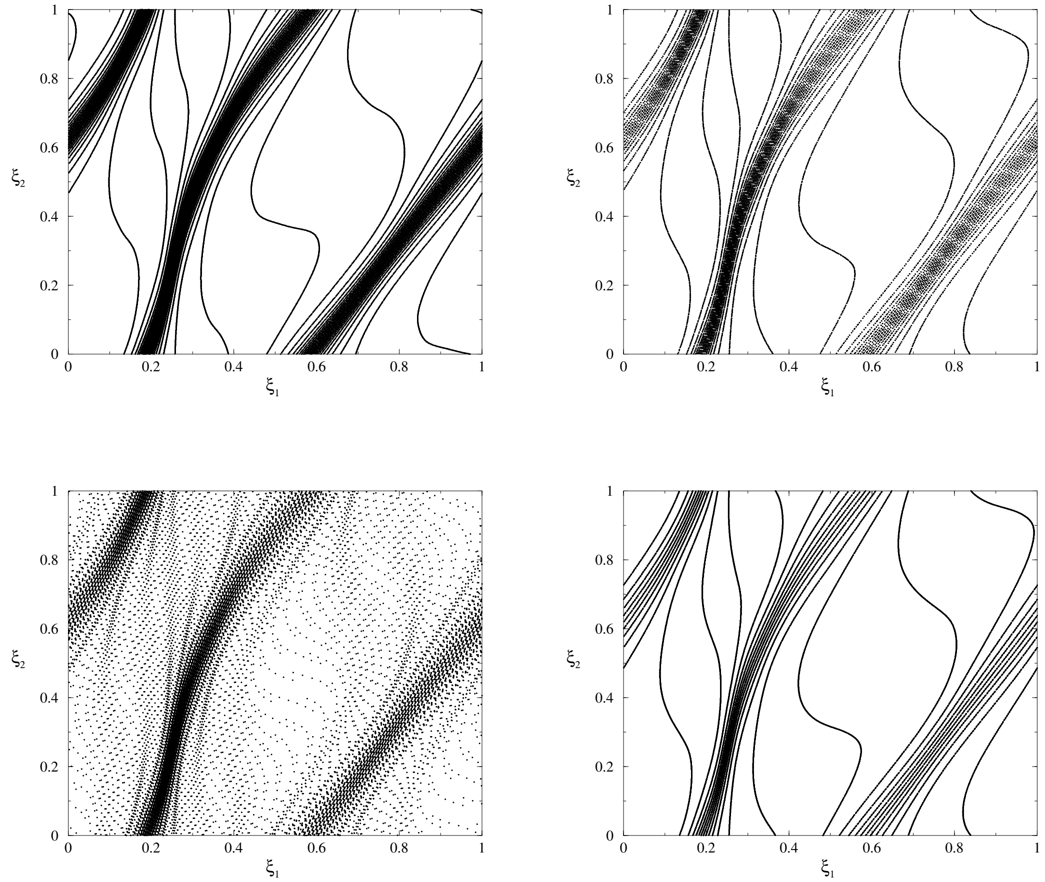

FIG. 8: Iterates of $\mathbf{g}$ for close values of the parameter α (all for $\beta = 0.13$, $\gamma = 0.2$). Clockwise, from top left: $\alpha = 0.6387$ – $(53, -23, 28)$-resonance, $\alpha = 0.6386$ – $(37, -15, 20)$-resonance, $\alpha = 0.6385$ – nonresonant, $\alpha = 0.6384$ – $(25, -9, 14)$-resonance.

eters – e.g., the $(4, 3, 4)$ and $(5, -1, 3)$ resonances for the map $\mathbf{g}$ occur for

$$\begin{aligned} \rho = \frac{4}{4 + 3\sigma_G} &= 0.683281572999747\ldots \\ \rho = \frac{3}{5 - \sigma_G} &= 0.684624205732747\ldots\ , \end{aligned}$$

respectively (where the meaning of ρ is the same as in (47)).

C. Numerical study of the resonant regions

Since the boundary of the resonance regions is particularly interesting (it is the region where the normal hyperbolicity breaks down), we have paid attention to computing them as accurately as possible.

1. Computation of the boundaries of a resonant region

We have adapted a method already used in [73] (see section 4.2 of that paper for more details and for the origins of the method) for one dimensional maps.

We use the fact that $\mathbf{g}$ preserves straight lines in the direction of $\boldsymbol{\omega}$. If $\mathbf{G}$ is a lift of $\mathbf{g}$, and $\mathcal{Z}_{\boldsymbol{\Xi}} := \{\boldsymbol{\Xi} + t\boldsymbol{\omega} | t \in \mathbb{R}\}$ is a straight line through $\boldsymbol{\Xi}$ in the direction of $\boldsymbol{\omega}$, then the map

$$\tilde{G} := \mathbf{G}|_{\mathcal{Z}_{\boldsymbol{\Xi}}} : \mathbb{R} \to \mathbb{R}$$

is 1-dimensional. Since $\sigma_G = \lim \frac{Q_{n-1}}{Q_n}$, where Q_n are the Fibonacci numbers, we approximate $\tilde{G}$ (for motion of the boundary given by (5), (6)) by the sequence of maps $\tilde{G}_n$ corresponding to motions of the boundary given by

$$a_n(t) := t + \frac{\alpha}{2} + \beta \left[\sin 2\pi t + \gamma \sin \left(2\pi \frac{Q_{n-1}}{Q_n} t \right) \right] .$$

The map $\tilde{G}_n$ is periodic of period Q_n, and if the map $\mathbf{g}$ is $(q, 0, p)$-resonant, $\tilde{G}_n$ has a periodic orbit of period qQ_n. We use a 1-dimensional zero finding routine `zbrent` to find $\alpha_{\pm}^{p,q,n}$, the ends of the intervals of α for which $\tilde{G}_n$ has a periodic orbit of period qQ_n. At the ends of these intervals of values of α, the map

$$t \mapsto \tilde{G}_n^{qQ_n}(t) - pQ_n$$

undergoes a tangent bifurcation.

It is empirically found that, increasing n, the $\alpha_{\pm}^{p,q,n}$ converge exponentially to a limiting value. This allows us to use Aitken extrapolation to compute the limiting values with a very high precision in a short time.

It is also empirically found that the values found are independent of the straight line $\mathcal{Z}_{\boldsymbol{\Xi}}$ we considered.

2. Numerical observations

One observation is that the boundaries of the resonant regions are – up to the precision of our computation – a smooth curves (except at a few points that we describe below). Since no straightforward application of either KAM theory or the theory of normally hyperbolic manifolds is seems apparent, this result does not seem obvious.

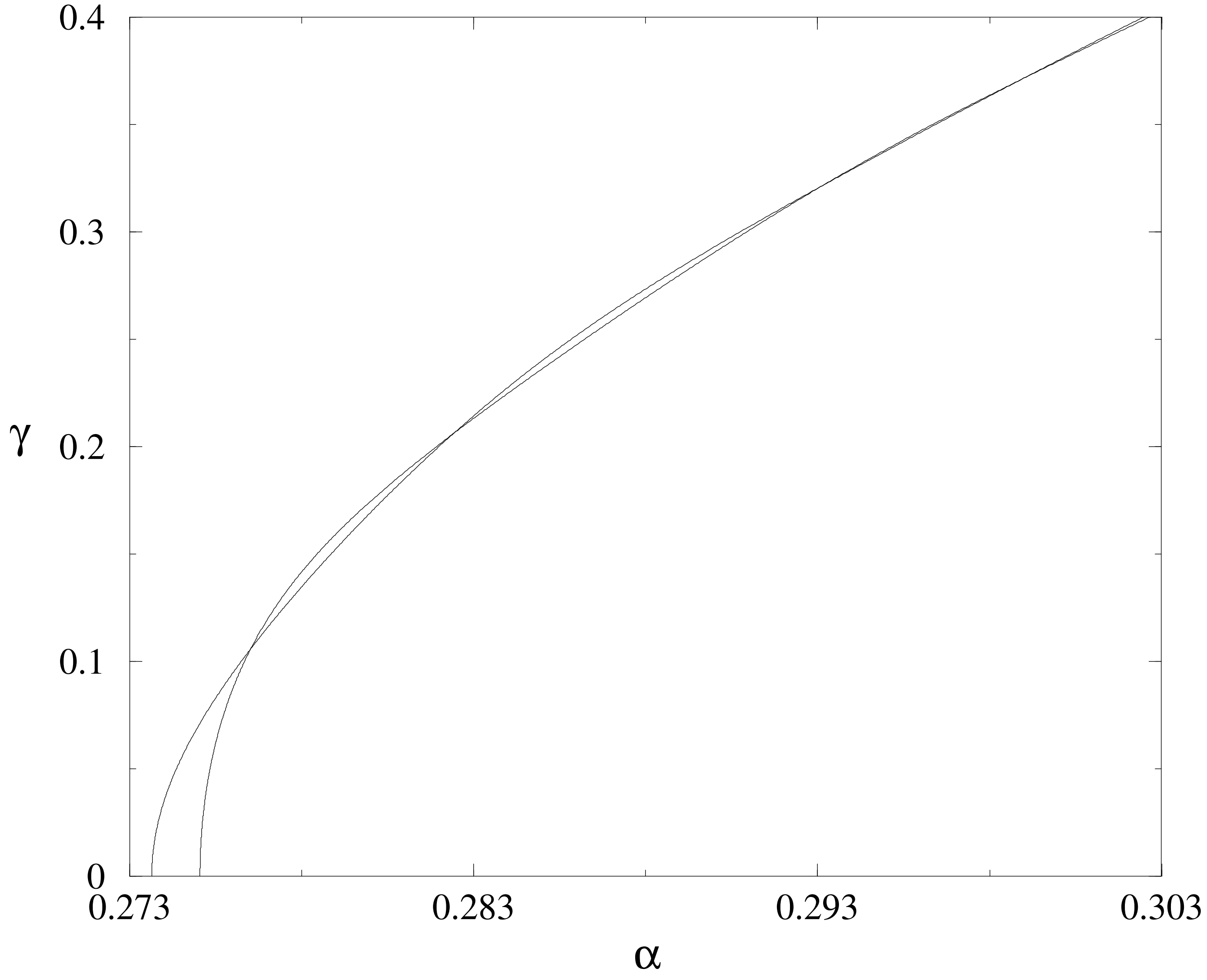

FIG. 9: Boundaries of the $\beta = 0.1$, $(5, 0, 1)$-resonant region in the (α, γ) plane.

More interestingly, we have found that some of the boundaries of resonance can be described as the intersections of smooth curves that cross over. These points of crossing are the places we alluded to in the previous paragraph where the boundaries are not smooth.

In Figure 9 we show the domain of parameters α and γ for which the map $\mathbf{g}$ is $(5, 0, 1)$-resonant with $\beta = 0.1$. As we see in the figure, the width of the interval of values of α for which the $(5, 0, 1)$-resonance occurs depends on the amplitude of the incommensurate forcing of the mirror (for the map $\mathbf{g}$ this incommensurate forcing is $\beta\gamma$).

It seems that the boundary seems can be described as the intersection of two smooth curves. To illustrate this phenomenon better, in Figure 10 we show the same phase locked region as in Figure 9, but "magnified", i.e., expanded proportionally around the "center

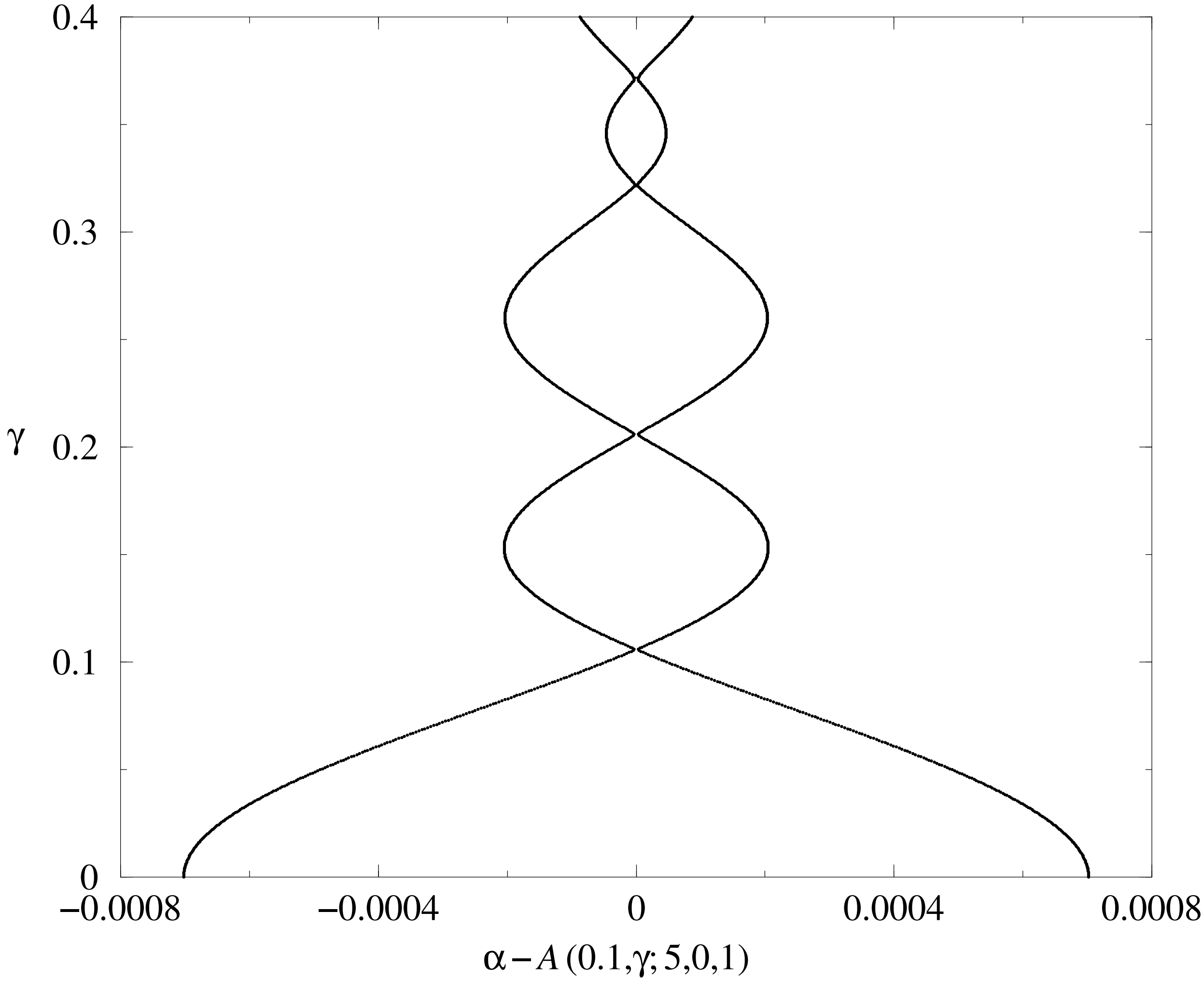

FIG. 10: "Magnified" plot of the resonant domain shown in Figure 9 – the domain is "straightened out" and expanded around its center line.

line" $A(0.1, \gamma;\, 5, 0, 1)$; here $A(\beta, \gamma;\, m_1, m_2, k)$ is the average of the two extreme values of α for which the map $\mathbf{g}$ is (m_1, m_2, k)-resonant for the particular values of β and γ.

Our numerical study shows that the width of the phase locked domain when "pinching" occurs is smaller than 10^{-9}, but we cannot say whether the "pinching" there is complete, i.e., whether the width of the phase-locked domain in the (α, γ) plane becomes zero.

The article [74] contains a study of the structure of the phase locked regions of another quasiperiodically forced circle map. We note that, in our case, the set of resonances is more complicated since a resonance in this case is indexed by three numbers rather that just by two.

"Pinching" does not occur for some resonances, for example for the $(3,0,2)$-resonance domain shown in Figure 5 – the $(3,0,2)$-resonance domain even becomes wider for larger values of γ. We do not know the reason for the different behavior of the resonant domains.

D. "Arnol'd tongues" in the case of quasi-periodic forcing

The regions where the phase locking in circle maps occurs are often called Arnol'd tongues. The name refers to the fact that, for two a two-parameter family of maps one of which is the rotation and another one the non-linearity, the phase locked regions look like thin wedges (tongues) in the region of small nonlinearity. See [75].

In the case of quasi-periodic maps, a very similar phenomena happens. The phase-locked regions form tongues and are described by a wedge in the region of small non-linearity. Studies of the generic quasi-periodic case can be found in [76].

For the families of mappings corresponding to motions of the boundary of the cavity described by the family (5), (6), the study of Arnol'd tongues amounts to describing the resonant region in the α-β while keeping γ fixed. The wedges appear in the region where β is small.

As we will see, the fact that the maps of the circle that we consider are non-generic also lead to the fact that the Arnol'd tongues in our case have quantitatively different properties from that of the generic case.

In Figure 11 we show in color (with the same color coding as in Figure 7) the resonant regions in the (α,β) plane for $\gamma = 0.4$, and in Figure 12, we show the same region of the (α,β) plane with the types of the resonance shown. (In Figure 12 the points (α,β) are shown if the Lyapunov exponent of the torus map for these values of α and β is smaller than -0.0001.)

Again, the structure of the (α,β) plane has a very rich structure – only one of the prominent resonances in these figures comes from an Arnol'd tongue existing in the unperturbed ($\gamma = 0$) case, namely the $(3,0,2)$ resonance coming from the $\frac{2}{3}$ locked circle map.

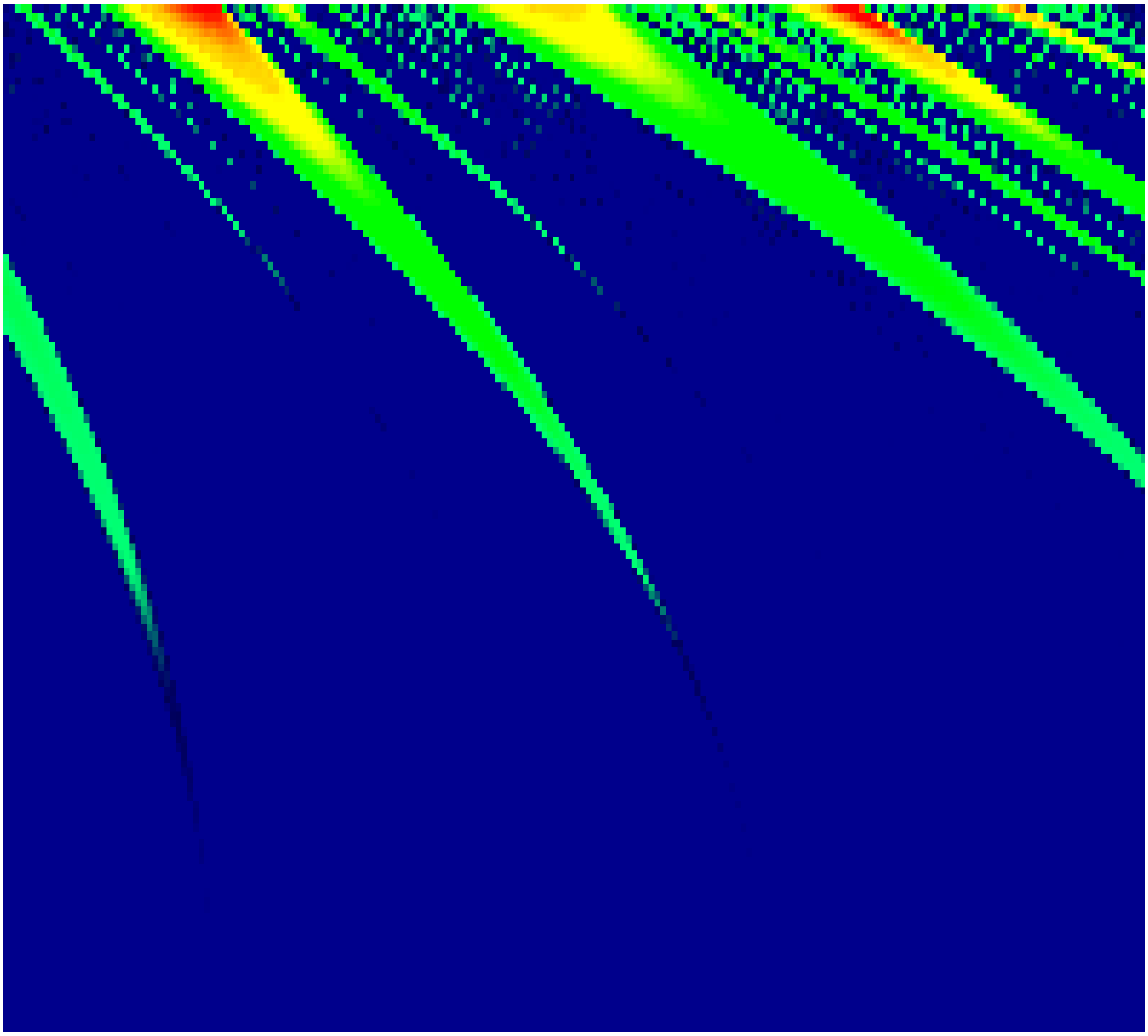

FIG. 11: Lyapunov exponents of the map $\mathbf{g}$ for $\gamma = 0.4$ in the (α, β)-plane for $\alpha \in [0.6, 0.7]$ (on the horizontal axis), and $\beta \in [0, 0.125]$ (on the vertical axis).

E. Occurrence of resonances absent for periodic motion of the mirror

In [5, Sec. IV D], it was emphasized that the family of circle maps occurring in the case of periodically pulsating cavity is non-generic. One of the manifestations of this nongenericity is the absence of phase locking with rotation number $\frac{1}{2}$. To illustrate this phenomenon, we show in Figure 13 the $(2, 0, 1)$-resonant domain (in the (α, γ)-plane) for $\beta = 0.1$. Note that in the unperturbed case ($\gamma = 0$), there is no phase locking with rotation number $\frac{1}{2}$, so the appearance of the $(2, 0, 1)$ resonance for $\gamma > 0$ is due to the incommensurate forcing.

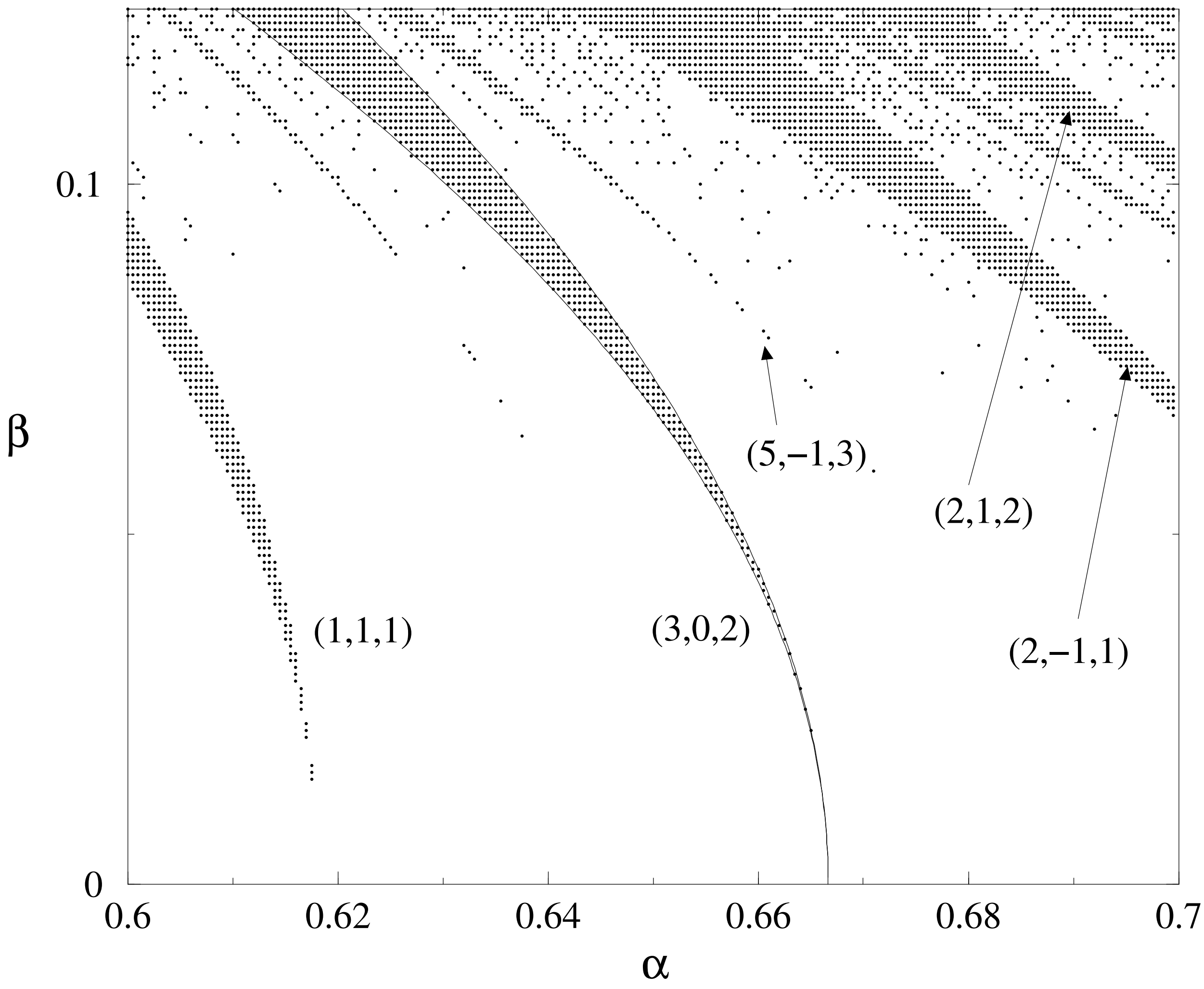

FIG. 12: Some of the most prominent phase resonant regions in the (α, β) plane for $\gamma = 0.4$.

In Figure 14, we show a log-log plot of the widths of the resonance regions (i.e., the length of the interval of α's corresponding to the resonance) as a function of β for fixed $\gamma = 0.4$. We see that for small β, the dependence is a power law.

The slopes of the lines in Figure 14 (i.e., the exponents in the power laws giving the width of the tongues as a function of the nonlinearity parameter β) were obtained using the linear regression facilities of xmgr and are given in Figure 15. Notice that many of these slopes appear to be – to very high precision – the ratios of small integers, and that all of them are larger than 1, in accordance to the general predictions of the theory in [21].

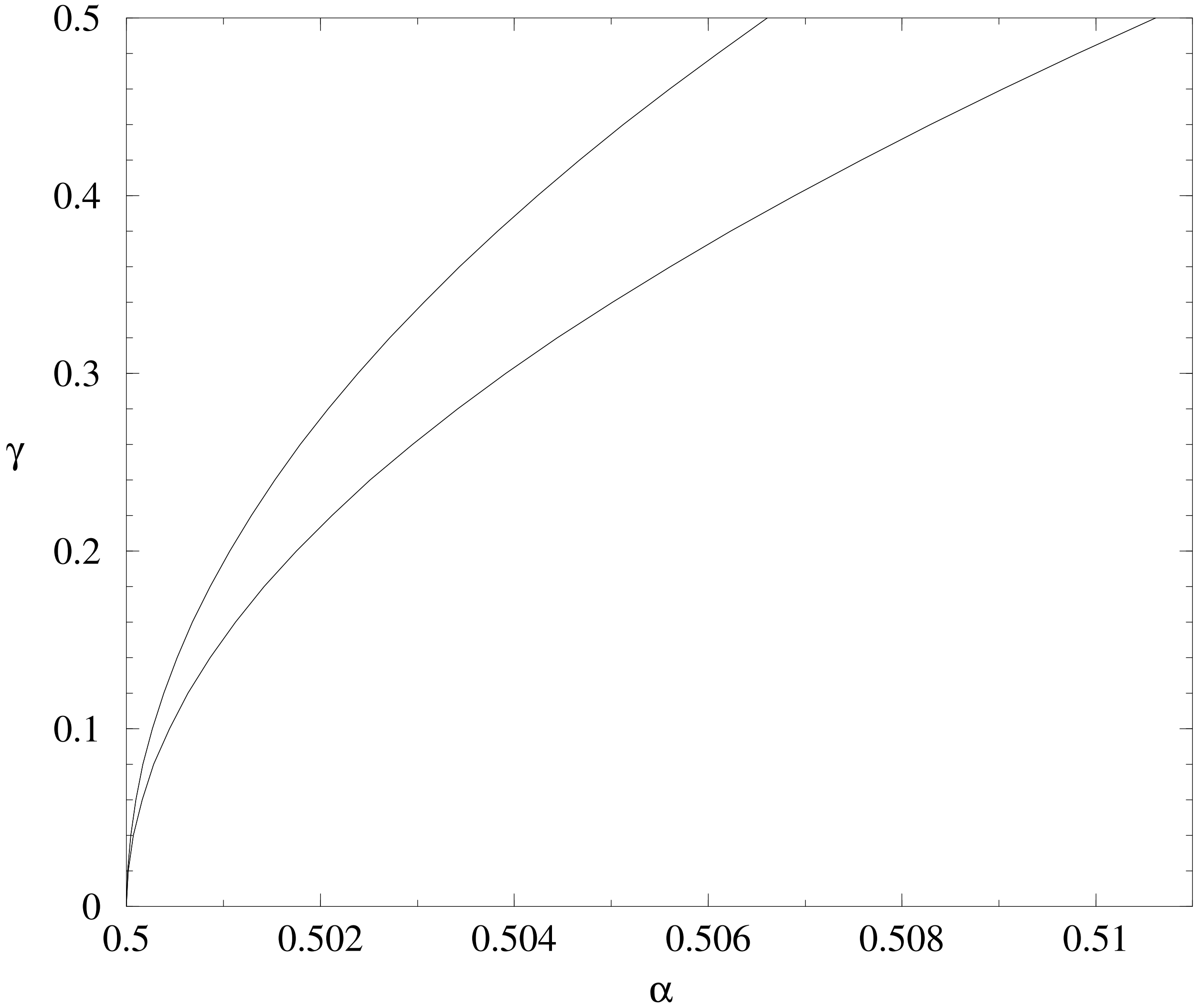

FIG. 13: An example of a resonance missing in the "unperturbed" case.

F. Rotations numbers and and Lyapunov exponent

In the previous sections, we have discussed how the existence of an attracting circle with a negative Lyapunov exponent implies that the rotation vector is locally constant (it should be a number satisfying some rational relations). We note also that, it is not difficult to show – see Remark III.13 – that, when the KAM theorem applies, most of the perturbations change the rotation number.

Hence, one expects that in numerical explorations (which only seem to see the KAM and the phase-locked regions), one would see the rotation number remaining constant precisely at the places where the Lyapunov exponent is negative.

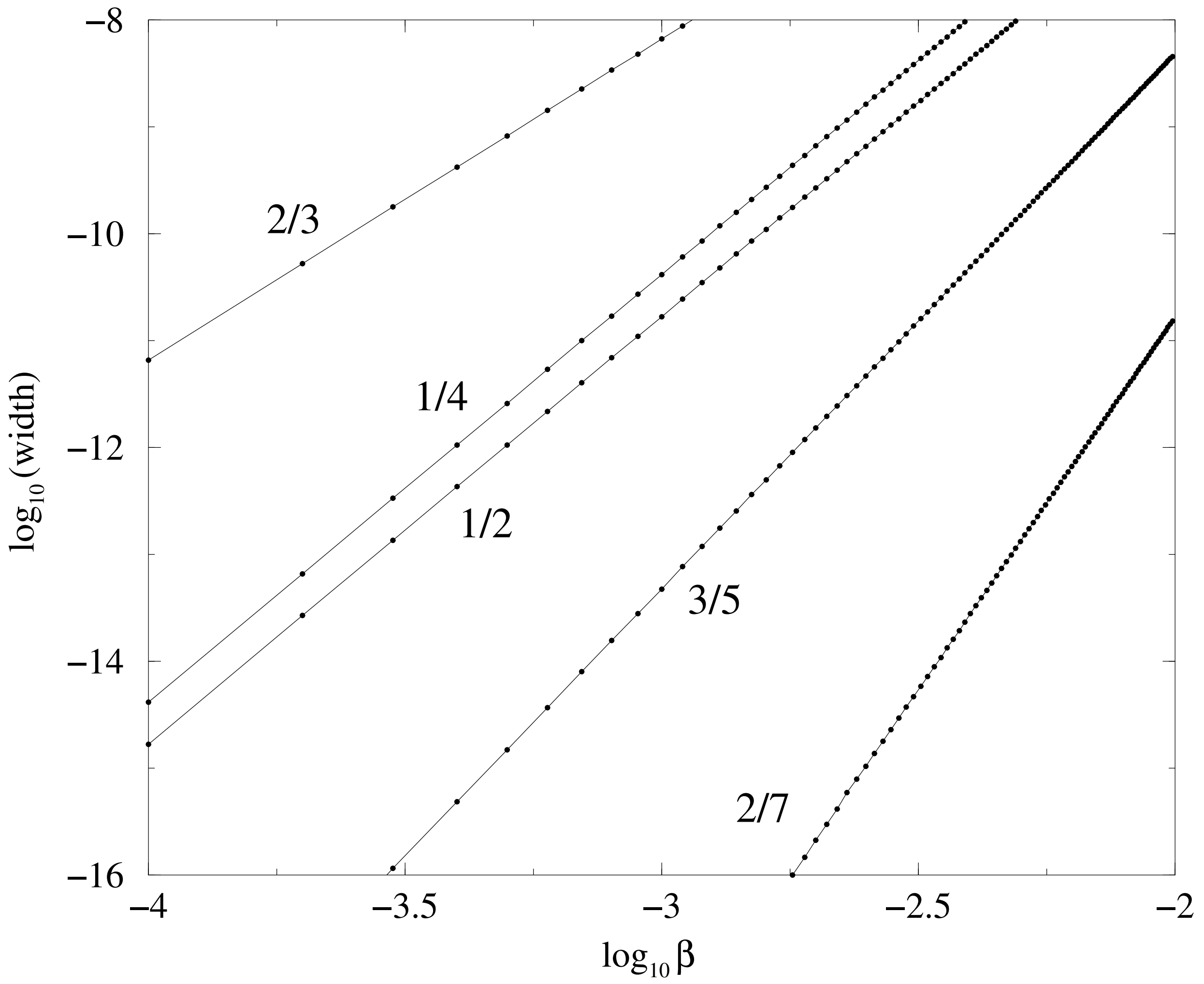

FIG. 14: A $\log_{10}$-$\log_{10}$ plot of the width of the "Arnol'd tongues" as a function of β for $\gamma = 0.4$. The types of the resonances are shown in the figure (3/5 means a resonance of type $(5, 0, 3)$).

Typical results of this exploration are depicted in Figure 16 where the thin line is the first component, ρ, of the rotation vector $\boldsymbol{\tau}(\mathbf{g})$ (see (47)), and the Lyapunov exponent of $\mathbf{g}$ as a function of α for $\beta = 0.13$, $\gamma = 0.2$. The scale on the vertical axis gives the values of ρ. The thick line is the Lyapunov exponent of $\mathbf{g}$ in arbitrary units, and shifted up by 0.79. The types of some resonances are shown. We see that the resonant domains occur for parameter values for which the Lyapunov exponent is negative. The values of β and γ used to make Figure 16 correspond to a horizontal line through the x's in Figure 5, and the "strong" resonances visible there can be seen clearly identified in Figures 5 and 7.

Moreover, the resonances of type $(q, 0, p)$ exist in the "unperturbed" ($\gamma = 0$) case, and

Resonance	**Slope**
$(2, 0, 1)$	3.999933
$(3, 0, 2)$	3.000002
$(4, 0, 1)$	3.998944
$(5, 0, 3)$	5.001203
$(7, 0, 2)$	6.983136
$(8, 0, 1)$	7.673007

FIG. 15: A table of the slopes of the linear regressions the various resonances appearing in Figure 14 (obtained using the linear regression facilities of xmgr).

in Figure 16 we see that they occur at rational values of ρ, namely, for $\rho = \frac{p}{q}$. On the other hand, the resonances that are due to the incommensurate forcing (i.e., of type (m_1, m_2, k) with $m_2 \neq 0$) occur at irrational values of ρ:

$$\rho = \frac{k}{m_1 + m_2 \sigma_G} \notin \mathbb{Q} .$$

We note that these calculations also agree with the calculations of the boundary of the resonance regions described in Section IV C 1. In Figure 12, we have depicted one of the boundaries computed by the method in Section IV C 1 as well as some of the regions computed by the Lyapunov method. The agreement is complete up to the uncertainties of the computation (which is much smaller than the pixels of the picture).

G. Power law dependence of the Lyapunov exponent near the boundary of resonances

The Lyapunov exponent near the resonances can be fit very well by a power law of exponent 1/2 near the boundary of resonance.

As a verification, we present an exploration for the same values of the parameters $\beta = 0.13, \gamma = 0.2$ considered in Figure 16. We computed, following the method indicated in Section IV C 1 that the left boundary of the $(3, 0, 2)$-resonance happens at $\alpha_L = 0.60505164827690$ – we think that all the figures are right –.

Figure 17 presents a plot of $\log(\mu)$ versus $\log(\alpha - \alpha_L)$. The regression fit yields an slope

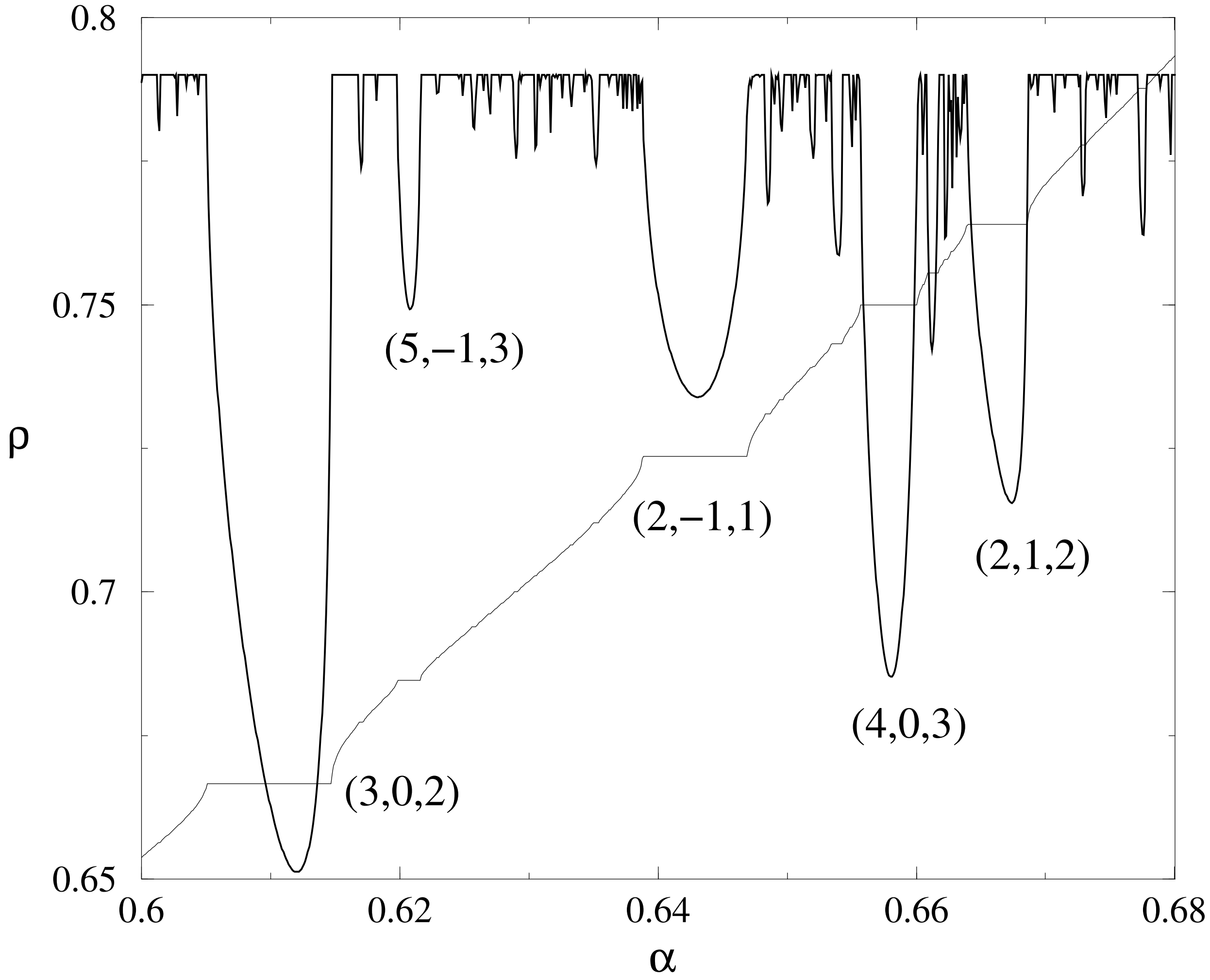

FIG. 16: Plot of the first component, ρ, of the rotation vector $\boldsymbol{\rho}(\mathbf{g})$, and the Lyapunov exponent of the map $\mathbf{g}$ as functions of α for $\beta = 0.13$, $\gamma = 0.2$.

of 0.4999969 with an standard error coefficient of $1.285733e-06$.

We think that this is strong evidence that one has a square root dependence of the Lyapunov exponent with respect to the bifurcation parameter. This suggests very strongly that the invariant circle is experiencing one (or some) of the standard bifurcations of invariant circles described in [77]. An analysis of these bifurcation for the maps of the form (25) is undertaken in [21].

Remark IV.2 *The agreement with the power laws in Figures 14 and 17 suggest that many of the possible terms in a perturbative expansion are absent and that, after the dominant one, there are quite a number of terms that are zero. This is related to the fact that our*

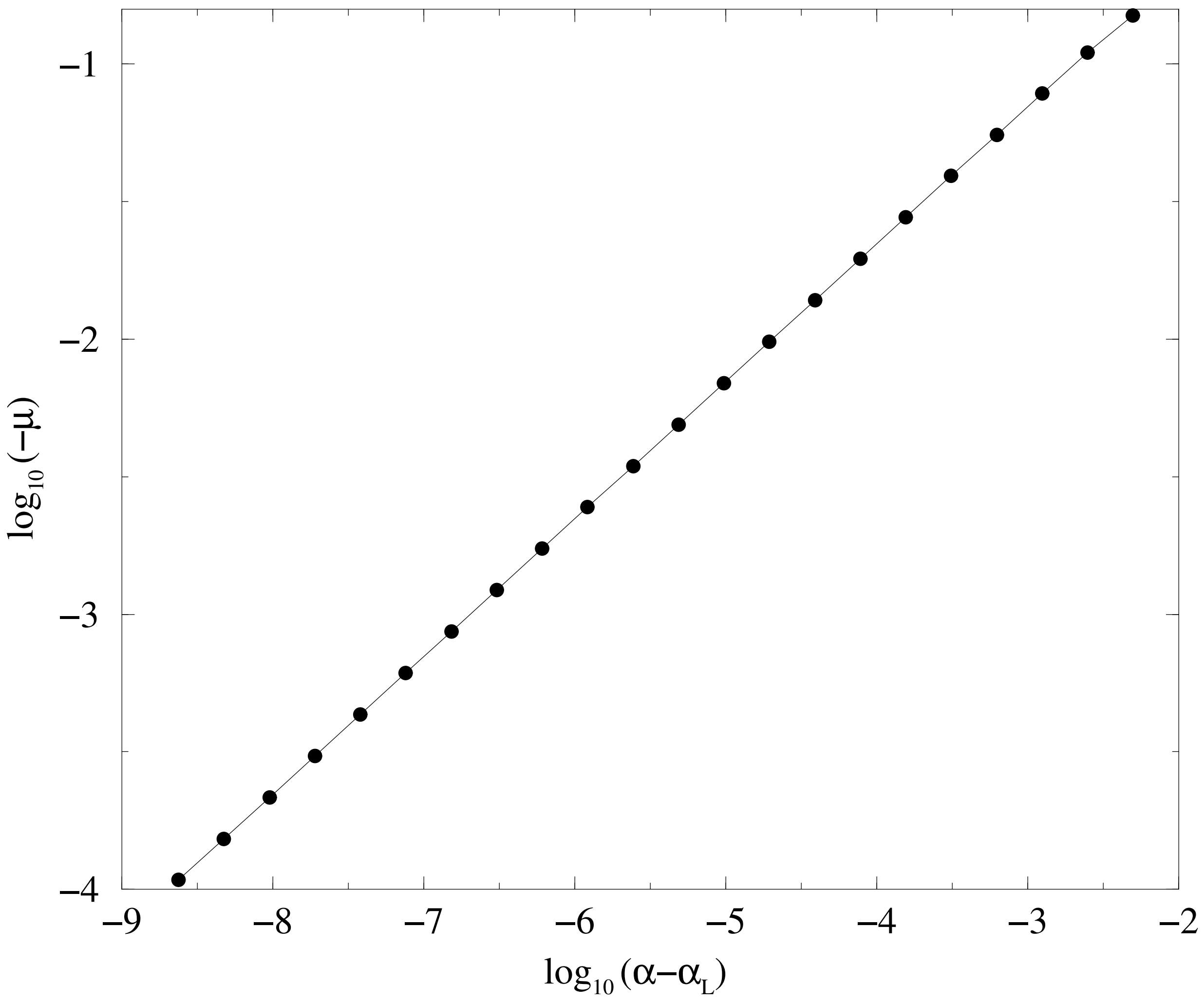

FIG. 17: Plot of $\log(\mu)$ vs. $\log(\alpha - \alpha_L$ for for $\beta = 0.13$, $\gamma = 0.2$.

perturbation has few harmonics.

V. CONSEQUENCES OF THE DYNAMICAL SYSTEMS PHENOMENA FOR THE FIELD IN THE RESONATOR

In this section we discuss how the dynamical results for torus maps (which were obtained rigorously or found numerically in the previous sections) imply results for the cavity problem.

In Sec. V A we briefly recall the results of [5] for a periodic motion of the mirror and explain their relation with the case of quasiperiodic motion.

In Sec. V B we derive a simple relationship between the asymptotic behavior of the Doppler factor for the physical system and the Lyapunov exponent of the torus map.

Sec. V C, explains our method for numerical computation of the energy density.

In Sec. V D and V E, we discuss the resonant and the KAM case, respectively.

Sec. V F gives a simple physical argument showing that, if one imposes Neumann boundary conditions instead of the "relativistic" ones (9), (10), then the energy of the field of the resonator will remain bounded and can *decrease* exponentially in the resonant case.

Finally, in Sec. V H we show how our methodology can be used to study the case of two periodically moving mirrors.

A. Comparison with the case of a periodically moving mirror

Let us start by recalling some of the results of [5] obtained for the case of a periodic motion of the mirror. In the case of phase locking, i.e., if the circle map has an attracting periodic orbit of period q, then the characteristics starting in a set of positive measure are attracted to this periodic orbit, so the electromagnetic field concentrates in q pulses of exponentially decreasing width and, hence, exponentially growing energy. Each of these narrow wave packets bounces back and forth between the two mirrors. The motion of the wave packets is asymptotically periodic – if the rotation number of the circle map is $\frac{p}{q}$, then the period of the motion of the wave packets is p.

In contrast, when KAM theory applies and reduces the circle map to a rotation, then the characteristics are well distributed and the electromagnetic field remains uniformly smooth and, hence, the electromagnetic energy remains uniformly smooth in time.

These two results have generalizations for maps of higher dimensional tori and imply results for the cavity pulsating quasiperiodically.

The analogue of the phase locking in the quasiperiodic case is the existence of a commensurate rotation vector with a uniformly attracting invariant set, which is a torus with a positive codimension, embedded in certain way into $\mathbb{T}^d$. If such a lower-dimensional attracting invariant torus exists, the iterates of the (d-dimensional) torus map quickly concentrate on the lower-dimensional torus, and asymptotically the dynamics happens within this lower-dimensional torus (this is illustrated for $d = 2$ in Figures 4 and 6). Furthermore, the nontrivial eigenvalue of $D\mathbf{g}$, i.e. λ given in (45), is negative and the energy of the system increases exponentially – for details see Section V B. The only essential difference with the case of a periodically moving mirror is that the motion of the wave packets is quasiperiodic.

In the quasiperiodic case when the KAM theorem applies the results are analogous to the case of a circle map, i.e. the energy of the system stays uniformly bounded in time (see Section V E).

B. Lyapunov exponent and Doppler factor

In Sec. II D we derived an expression for the Doppler factor, $\mathcal{D}(\theta)$ (17), at reflection from the moving mirror at time θ. Here we derive an expression of the asymptotic behavior of the rate of change of the energy of the field.

Let one particular characteristic "ray" be reflected from the moving mirror at times θ_0, θ_1, θ_2, …, and let $\boldsymbol{\xi}_n \equiv \mathbf{\Pi}(\boldsymbol{\omega}\theta_n)$ be the vectors of the phases of the mirror's motion at the moments of reflection. By the definition of the corresponding torus map $\mathbf{g}$ (23), $\boldsymbol{\xi}_n$ are iterates of $\mathbf{g}$:

$$\boldsymbol{\xi}_n = \mathbf{g}(\boldsymbol{\xi}_{n-1}) = \cdots = \mathbf{g}^n(\boldsymbol{\xi}_0) \ .$$

Using the expression for the nontrivial eigenvalue, λ, of $D\mathbf{g}$ given in (45) of Sec. III G, we obtain for the only nontrivial Lyapunov exponent of $\mathbf{g}$

$$\begin{aligned}
\mu &\equiv \lim_{N\to\infty} \frac{1}{N} \log \prod_{n=1}^{N} \lambda(\boldsymbol{\xi}_n) \\
&= \lim_{N\to\infty} \frac{1}{N} \log \prod_{n=1}^{N} \frac{1+\boldsymbol{\omega}\cdot\nabla\Phi(\boldsymbol{\xi}_n)}{1-\boldsymbol{\omega}\cdot\nabla\Phi(\boldsymbol{\xi}_{n+1})} \\
&= \lim_{N\to\infty} \frac{1}{N} \log \prod_{n=1}^{N} \frac{1+\boldsymbol{\omega}\cdot\nabla\Phi(\boldsymbol{\xi}_n)}{1-\boldsymbol{\omega}\cdot\nabla\Phi(\boldsymbol{\xi}_{n})} \\
&= -\lim_{N\to\infty} \frac{1}{N} \log \prod_{n=1}^{N} \mathcal{D}(\theta_n) \\
&= -\lim_{N\to\infty} \frac{1}{N} \sum_{n=1}^{N} \log \mathcal{D}(\theta_n) \ .
\end{aligned} \tag{49}$$

Let T be the mean transit time defined in (26). Note that, for our choice of the frequency vector $\boldsymbol{\omega}$ (6), the first component of the rotation vector $\boldsymbol{\tau}(\mathbf{g})$ (defined in (47)) is equal to the fractional part of T. This means that asymptotically, in a time interval of length NT, the energy E changes by a factor of $\prod_{n=1}^{N} \mathcal{D}(\theta_n)$. Therefore, in a unit time interval, $\log E$

increases on average by

$$\frac{1}{T}\frac{1}{N}\log\prod_{n=1}^{N}\mathcal{D}(\theta_n) \approx -\frac{\mu}{T} \; .$$

Taking all this into account, we obtain

Proposition V.1 *The only nontrivial Lyapunov exponent* μ *of the torus map* $\mathbf{g}$ *is equal to the negative of the average over a trajectory of the logarithm of the Doppler factor at reflection from the moving mirror:*

$$\begin{aligned} \mu &= -\left\langle \log \mathcal{D}(\theta_n) \right\rangle_{\text{averaged over } n} \\ &:= -\lim_{N\to\infty}\frac{1}{N}\sum_{n=1}^{N}\log\mathcal{D}(\theta_n) \; . \end{aligned}$$

If the initial conditions of the boundary value problem for the vector potential A *are continuous, then the asymptotic behavior of the energy of the electromagnetic field is given by*

$$E(t) \sim E(0)\exp\left(-\mu\frac{T}{t}\right) \; .$$

C. Method for computing the energy density

Before we discuss the resonance and the KAM cases in Sections V D and V E, let us explain how we compute the pictures of the evolution of a wave packet given in these sections.

The main idea is to use the methods of characteristics in order to avoid solving partial differential equations. We used the fact that the energy density of the electromagnetic field is proportional (up to an overall factor) to the spatial density of the characteristics. We take into account that at each reflection the electromagnetic field changes sign, so to find the density of the energy of the field in a small spatial interval $[x_1, x_2]$ at a particular moment t, we subtracted the number of characteristics going through the line connecting the points (t, x_1) and (t, x_2) on the space-time diagram and going to the left from the ones passing through this line and going to the right, and took the absolute value of the difference. We note that this algorithm is very similar to ray tracing in computer graphics and is quite parallelizable.

To produce Figures 18, 19, and 20, we used 2^{20} rays (with initial density corresponding to the initial energy density of the wave packet) and studied their distribution in 2^{12} bins.

D. The resonant case

In the case when there exists a uniformly attracting invariant torus (the fact that this situation indeed happens is suggested by Theorem III.3 and by numerical explorations), one can make somewhat more precise predictions for the behavior of the electromagnetic field.

Lemma V.1 *Let* $\mathbf{g}$ *be a map of the form* (23) *describing a cavity with quasiperiodically moving boundary as in Sec. II E. Assume that* $\mathbf{g}$ *has an invariant torus* $\mathcal{L}$ *of type* $(\mathbf{k}, n)$*, which is uniformly attracting (Def. III.5) with exponent* μ*, and average crossing time* T*. Let the initial condition (which we assume is not identically zero) be supported on the basin of attraction of* $\mathcal{L}$*.*

Then $A(t,x)$ *consists of a pulse of width decreasing exponentially with exponent* μ/T*. The energy of the pulse is increasing exponentially with exponent* μ/T*.*

The support of the pulse contains a characteristic $\mathcal{C}$ *whose intersecting phases on the right mirror move quasiperiodically along the torus* $\mathbb{T}^d$ *with frequency* $\boldsymbol{\omega} \cdot \mathbf{k}$*.*

In the case that the map $\mathbf{g}$ *is defined on the two dimensional torus and* $\mathcal{L}$ *is one-dimensional, we can use the mapping* Ψ *of Lemma III.3 to find a characteristic* $\mathcal{C}$ *and an analytic systems of coordinates* $x'_n(x)$*, define near the regions of space-time where* $\mathcal{C}$ *intersects with the boundary of the cavity, such that:*

- *Each of the derivatives of the changes of variables are bounded uniformly in* n*.*
- *The characteristic* $\mathcal{C}$ *corresponds to* $(t = t_n + \Delta, x'_n = 0)$*. The characteristics close to* $\mathcal{C}$ *that reflect slightly after* t_n *have coordinates* $t = t_n + \Delta, x'_n < 0$*, those that reflect slightly afterwords have coordinates* $t = t_n + \Delta, x'_n > 0$*.*
- *Given a characteristic of coordinates* $t_n + \Delta, x'_n$*, it also goes trough the coordinates* $t_{n+1} + \Delta, x'_n$*.*

Proof. Recall that the map $\mathbf{g}$ describes the characteristics at the time of collision with the moving boundary. The assumption implies that the characteristics emanating from within the support of the initial conditions are getting exponentially contracted under the map $\mathbf{g}$.

As a consequence, the times of collision with the moving mirror of each of the characteristics are also getting exponentially close. From this it follows that the time of collision with the characteristics is concentrated in an interval of exponentially decreasing width and hence the support of the electromagnetic wave decreases exponentially with time.

The argument for the growth of the energy is given in Sec. V B.

As for the use of the coordinate map to construct the coordinate system, note that if we fix Δ sufficiently small, we can find a one-to-one correspondence δ_n between the point in the line given by $t = t_n + \Delta$ and the time at which the n^{th} reflection of the characteristic $\mathcal{C}$ occurs (i.e. the time at which $\mathcal{C}$ intersects the boundary of the cavity). If the motion of the boundary is analytic, these correspondences δ_n are analytic with uniform bounds in n.

Since the mapping Ψ gives a coordinate on a neighborhood of $\mathcal{L}$, in particular this allows us to obtain coordinates in neighborhoods of the points where $\mathcal{C}$ intersects the boundary, i.e. in neighborhoods of $\mathcal{C} \cap \{t = t_n + \Delta\}$. These coordinates will be uniformly analytic and the uniformity of the contraction follows from (b.2) in Lemma III.3. $\square$

From the point of view of direct observations, this means that, if the hypotheses of Lemma V.1 are met, we will see that the electromagnetic field will concentrate in lumps and that the center of the lumps will move quasiperiodically along the cavity (up to an exponentially decreasing error).

In Figure 18, we show the evolution of a wave packet in the resonance case. The parameters of the mirror's motion are $\alpha = 0.61$, $\beta = 0.13$, $\gamma = 0.2$ (this point is shown in Figure 5), and for these parameter values the torus map $\mathbf{g}$ is $(3, 0, 2)$-resonant. At the initial moment ($t = 0$), the wave packet was supported on the interval $x \in [0.03, 0.24]$, and was moving to the right. The figure shows the energy density of the electromagnetic field at times $t = 0$, $\frac{2}{3}$, $\frac{4}{3}$, …, $\frac{58}{3}$. The wave packet splits in two wave packets, and these two wave packets become narrower and higher with time at a rate that is asymptotically exponential. This is especially clear if one looks at the density at the moments shown with thick line. The fact that the associated torus map $\mathbf{g}$ is $(3, 0, 2)$-resonant means that, asymptotically, the motion of the wave packets is such that at some particular moment t the positions of the wave packets is close to their positions at time $t - 2$ (in terms of the torus map, this means that a point from some attractive invariant circle, iterated 3 times, comes to the same invariant circle – see more details below). This is the reason for drawing every third snapshot with a thick line – the elapsed time between two adjacent such snapshots is 2 seconds.

To understand better why this happens, we show in Figure 19 the evolution of the wave

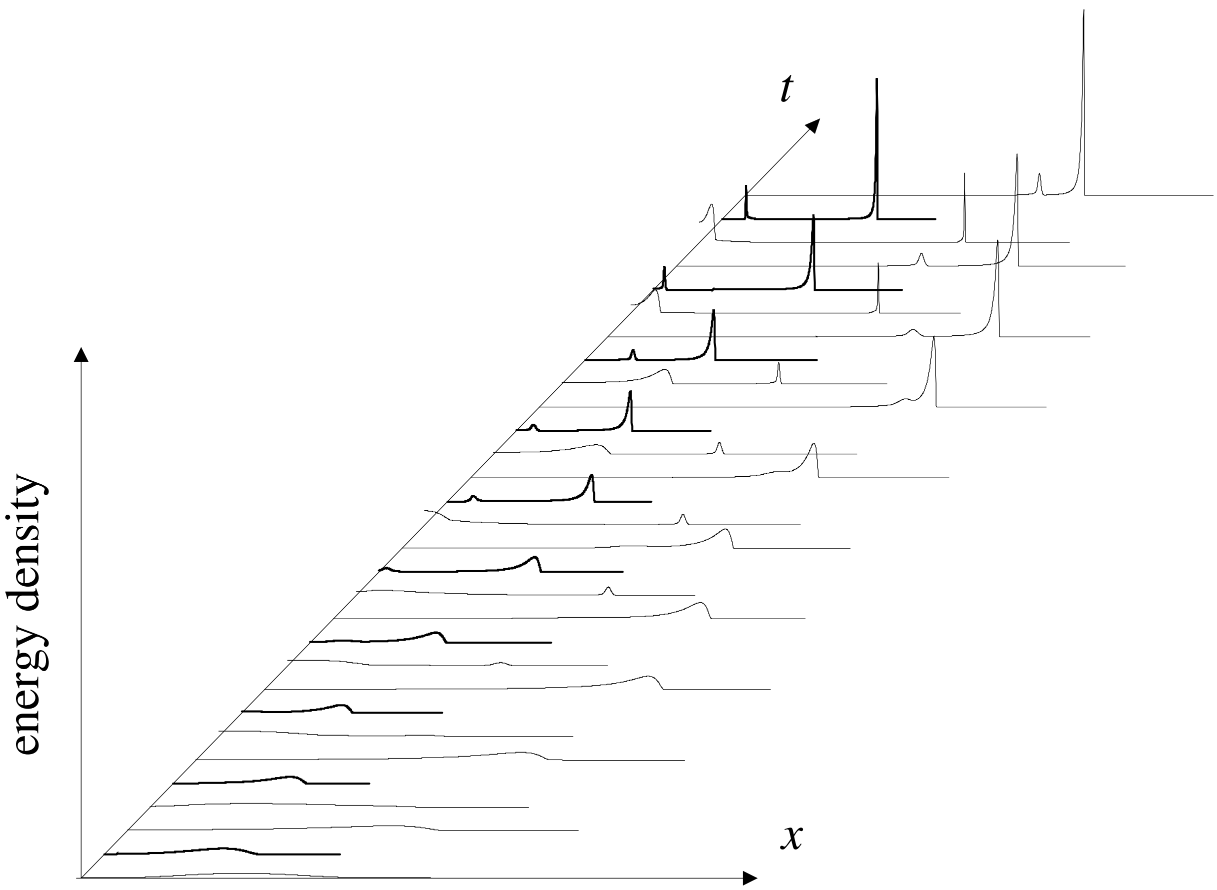

FIG. 18: Evolution of a wave packet in a $(3, 0, 2)$-resonant case.

packet, shown as the motion of the iterates of the associated torus map $\mathbf{g}$ in $\mathbb{T}^2$. To produce this figure, we took 22 points,

$$x^{(1)} = 0.03\ , \quad x^{(2)} = 0.04\ , \quad x^{(3)} = 0.05\ , \quad \ldots\ , \quad x^{(22)} = 0.24\ ,$$

equidistributed on the support of the wave packet from Figure 18 at the initial moment $t = 0$. First we found the time θ_0^k ($k = 0$, 1, ..., 22) of the first reflection from the moving mirror of the right-moving characteristic emanating from each point $x^{(k)}$ at $t = 0$ (i.e., from the point $(0, x^{(k)})$ in the space-time diagram). These times are represented in the figure by the points $\boldsymbol{\xi}^{(k)} := \boldsymbol{\Pi}(\boldsymbol{\omega}\theta_0^{(k)}) \in \mathbb{T}^2$ and are labeled by 22 circles with the number 0 to their left. Then we illustrated the evolution of these points by showing their 3rd iterates $\mathbf{g}^3(\boldsymbol{\xi}^{(k)})$ (labeled by the squares near the 3), their 6th iterates $\mathbf{g}^6(\boldsymbol{\xi}^{(k)})$ (labeled by the diamonds near the 6), their 9th iterates $\mathbf{g}^9(\boldsymbol{\xi}^{(k)})$ (labeled by triangles near the 9), ..., their 27th iterates $\mathbf{g}^{27}(\boldsymbol{\xi}^{(k)})$ (labeled by the stars near the 27).

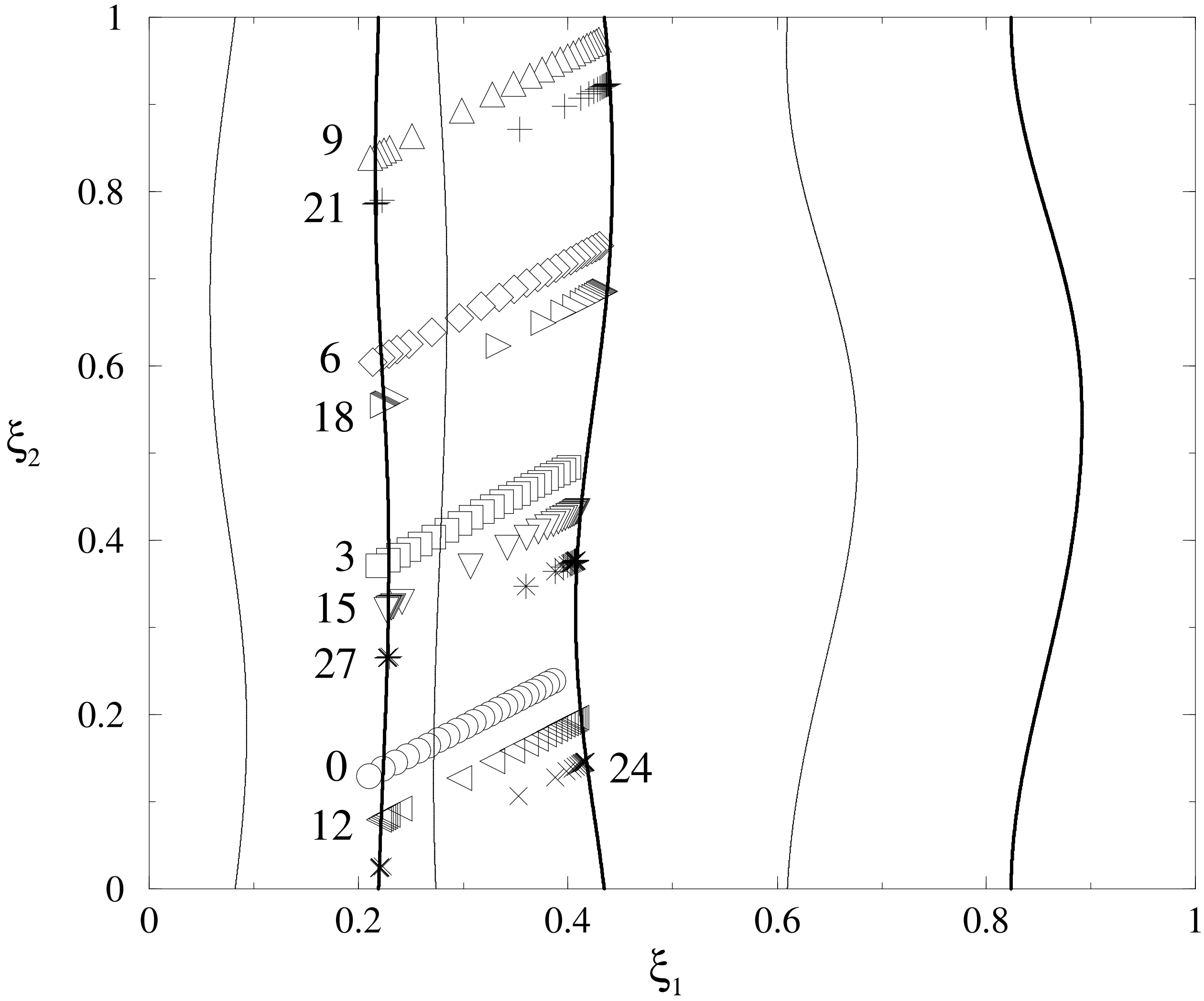

FIG. 19: Evolution of the wave packet of Figure 18, depicted as iterates under $\mathbf{g}^{3n}$ of points from the support of the wave packet at $t = 0$.

The map $\mathbf{g}$ for these values of the parameters of the mirror's motion is $(3, 0, 2)$-resonant, and its attracting invariant circles are shown with thick lines in the figure, while the repelling ones are represented with thin lines. The points $\boldsymbol{\xi}^{(k)}$ (the circles) belong to the basins of attraction of the first and the second from the left invariant circles in the figure, six points being in the basin of attraction of the leftmost one. These six points are being attracted to the leftmost invariant circle, and the others are being attracted to the other invariant circle. From Figure 19, it is very clear how the points are being pushed away from the repelling invariant circle and accumulate on the attractive ones, which means that the electromagnetic field forms two packets with exponentially growing energy. For these parameter values, the electromagnetic field can form up to three wave packets – the actual number of the wave packets depends on the support of the electromagnetic field at $t = 0$. (Here we assume that initially the electromagnetic vector potential is continuous – otherwise, if the electromagnetic potential that is initially supported on a point, it may turn out that this point corresponds to a point in $\mathbb{T}^2$ that belongs to the unstable manifold.)

E. The KAM case

In contrast with Sec. V D, we have the following

Lemma V.2 *Assume that the map* $\mathbf{g}$ *is* C^r *conjugate to a translation (e.g., when the KAM theorem applies).*

Then, given any C^r *initial data, the* C^r *norm of the electromagnetic field remains uniformly bounded for all time.*

In particular, when $r \geq 1$*, the energy of the electromagnetic field remains bounded for all time.*

Remark V.1 *We note that, according to Theorem III.2, given a family of motions, the behavior described in Lemma V.2 will happen in Cantor sets of parameters of large measure.*

Typically, in the gaps of these Cantor sets there are intervals for which Theorem III.3 applies. Hence, we have that for the physical problem, situations with unbounded energy and with bounded energy are intimately mixed in the space of parameters.

Proof. We note that $\mathbf{g} = \mathbf{h}^{-1} \circ \mathbf{t}_{\boldsymbol{\tau}(\mathbf{g})} \circ \mathbf{h}$ yields $\mathbf{g}^n = \mathbf{h}^{-1} \circ \mathbf{t}^n_{\boldsymbol{\tau}(\mathbf{g})} \circ \mathbf{h}$, therefore (taking into account that $D\mathbf{t}_{\boldsymbol{\tau}(\mathbf{g})} = \mathrm{Id}$)

$$D\mathbf{g}^n = (D\mathbf{h}^{-1} \circ \mathbf{t}^n_{\boldsymbol{\tau}(\mathbf{g})} \circ \mathbf{h}) \cdot (D\mathbf{h}) \ .$$

Hence

$$\|D\mathbf{g}^n\|_{C^0} \leq \|D\mathbf{h}^{-1}\|_{C^0} \, \|D\mathbf{h}\|_{C^0} \leq \|\mathbf{h}^{-1}\|_{C^1} \, \|\mathbf{h}\|_{C^1} \ .$$

More generally, we obtain (for C depending on r and d only)

$$\|D^r\mathbf{g}^n\|_{C^0} \leq C \, \|\mathbf{h}^{-1}\|_{C^r} \, \|\mathbf{h}\|_{C^r} \ .$$

Once we have that $\mathbf{g}^n$ is uniformly C^r, we observe that the map that gives the position of the characteristic at time θ is obtained by composing $\mathbf{g}^n$ with a map which gives the solution from the time of the last reflection to θ.

Since the last reflection happens not more than $2\max_t a(t)$ units of time before θ (independent of what t is), $\|D^r\mathbf{g}^n\|_{C^0}$ is uniformly bounded.

Once we have that the characteristics give rise to a uniformly smooth map, the result follows.

For the left propagating characteristic, we perform a similar argument. $\square$

In Figure 20, we show the evolution of a wave packet for motion of the mirror that corresponds to the KAM case, for $t = 0$, 500, 1000, 1500, 2000, 2500, 3000, and 3500. At $t = 0$, the wave packet is moving to the right. On the vertical axis we give the energy density in arbitrary units. We see that, although the shape of the wave packet changes, its energy stays bounded. The shape of the packets for different t is different, although this cannot be clearly seen in the picture.

F. On the role of the boundary conditions

Here we would like to give simple physical arguments showing that Neumann boundary conditions lead to very different predictions than the relativistic ones (9), (10).

First note that the relativistic boundary conditions, (9), (10) are equivalent to the Dirichlet ones,

$$A(t,0) = \text{const} \ , \quad A(t,a(t)) = \text{const} \ . \tag{50}$$

Therefore, the procedure for constructing the solution described in Section II C can also be applied for Dirichlet boundary conditions.

However, for Neumann boundary conditions the situation is different. To see why, let us consider the wave equation (7) with Neumann boundary conditions

$$A_x(t,0) = 0 \ , \quad A_x(t,a(t)) = 0 \ , \tag{51}$$

and initial conditions (11).

The most important observation is that by setting $u := A_x$, we transform the Neumann

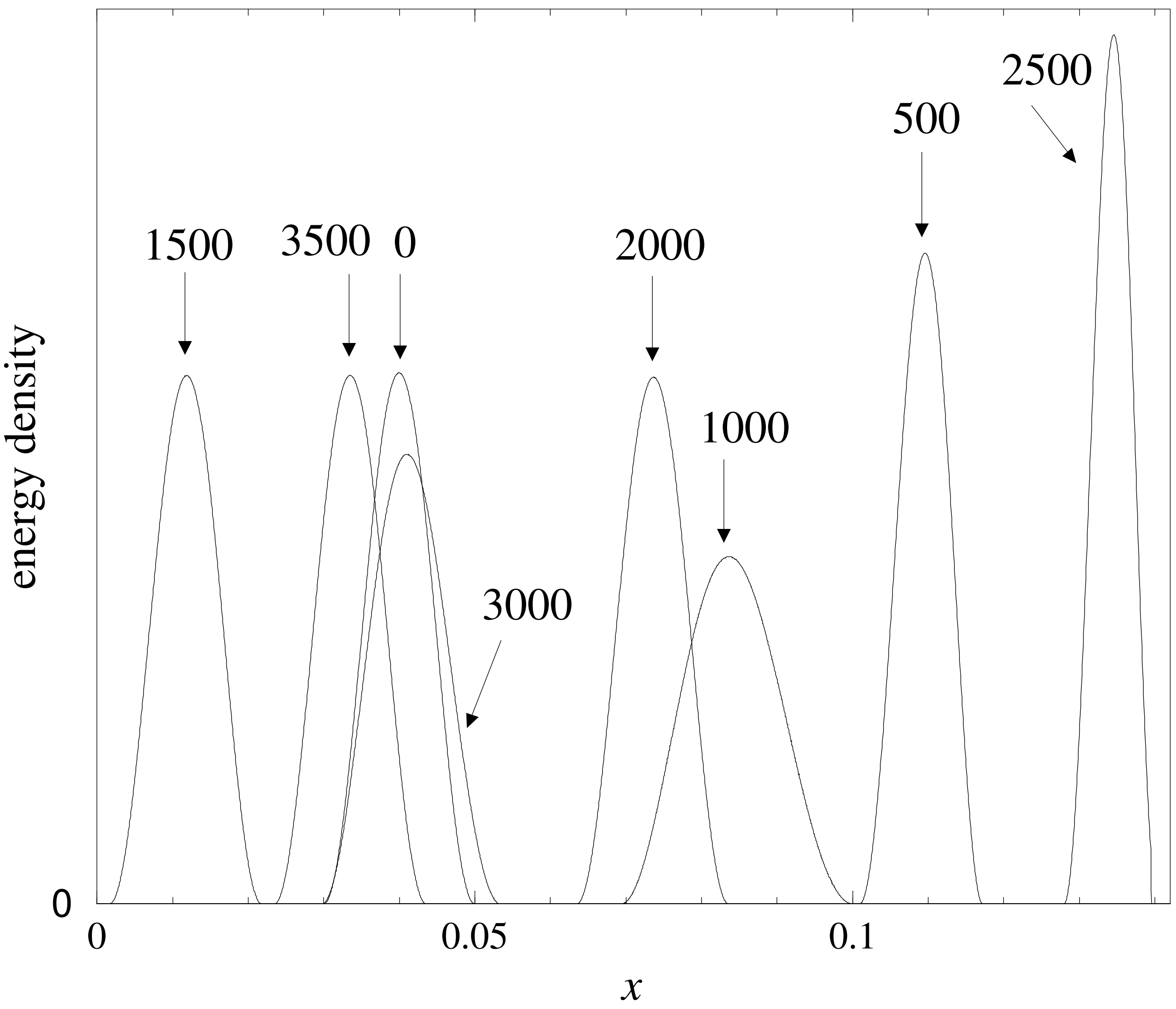

FIG. 20: Evolution of a wave packet in the KAM case.

boundary value problem (7), (51), (11) into the Dirichlet boundary value problem

$$
\begin{aligned}
&u_{tt}(t,x) - u_{xx}(t,x) = 0\ , && (t,x) \in \Sigma\ ,\\
&u(0,x) = \psi_1'(x)\ ,\quad u_t(0,x) = \psi_2'(x)\ , && x \in (0,a(0))\ ,\\
&u(t,0) = 0\ ,\quad u(t,a(t)) = 0\ , && t \geq 0\ ,
\end{aligned}
\tag{52}
$$

which can be solved by applying our method from Section II C.

Recall that the reason for the energy growth in the case of relativistic or Dirichlet boundary conditions is the change of the distance between rays at reflection from the moving mirror, as shown in Figure 2. At the same time, the absolute value of the solution does not change at reflection. The effect of this is to increase the first derivatives (in x and t) of u by a factor of $\mathcal{D}(\theta)$ while decreasing the spatial distances by a factor of $\mathcal{D}(\theta)$ which results in an overall increase in the energy (18) by a factor of $\mathcal{D}(\theta)$, where $\mathcal{D}(\theta)$ is the Doppler factor at reflection at time θ (see Sections II D).

To simplify the exposition, let us consider only the case of motion of the boundary for which the system is in a phase locking regime. Note that whether the system is phase locked does *not* depend on the boundary conditions, but only on the behavior of the characteristics (which in turn depends on the motion of the mirror). In this case the solution of the Dirichlet boundary value problem (52) will develop wave packets whose width will decrease exponentially in time. Note that for long enough times, when the wave packets are well separated, the solution $u(t,x)$ at each moment (except during the short periods of time when a wave packet undergoes a reflection) consists of *unidirectionally moving* wave packets. In general, the energy of the solution $A(t,x)$ of the Neumann boundary value problem (7), (51), (11) cannot be simply expressed in terms of the function u, but for unidirectionally moving wave packets it is approximately equal to

$$E(t) = \int_0^{a(t)} u(t,x)^2 \, dx \ . \tag{53}$$

To write (53), we neglected the overlap between different wave packets, and used the fact that for unidirectionally moving $A(t,x)$, the relations $A_t(t,x) = \pm A_x(t,x)$ hold (the sign depending on the direction of the motion). We see that in a phase locking regime the wave packets of the field u, whose energy is given by (53), will become narrower at exponential rate, while the field u will only change sign at reflection, hence the integral of the square of u will *decrease* at exponential rate.

This simple physical argument shows that the behavior of the solutions of the relativistic (or Dirichlet) and the Neumann boundary value problems in a pulsating spatial domain behave very differently, the most dramatic difference being that in phase locking the energy of the former *increases* exponentially, while the energy of the latter *decreases* exponentially. The main reason for this is that the expression for the energy of a solution of the Neumann boundary value problem can be written in the form (53) which does not contain derivatives.

Similar phenomena have been previously noticed in [78], where the authors noticed that (in a slightly different context) the solutions may tend to zero in some Sobolev norms, but grow in others (see Section 2 and the end of Section 1 of [78]), and in [18]. The novelty of our approach is in giving an intuitively clear explanation of the phenomenon by linking it with the behavior of the characteristics of the wave equation.

It is worth mentioning the old work [26], in which the motion of a string with one moving end was considered, and the rate of increase of the energy was related with the work the wall performs on the moving end.

G. Evolution of other conserved quantities of the wave equation in the line

Besides the energy, the wave equation in the line preserves other quantities. Notably, if u solves the wave equation in the line, and is propagating in one direction, then

$$I_{k,s}(u) \equiv \left(\int_{\mathbb{R}} |\partial_x^k u(x)|^s \right)^{1/s} \tag{54}$$

remains constant under the time evolution. As usual, $I_{k,\infty}$ means taking the essential supremum. Note we have – Minkowski's inequality –

$$I_{k,s}(u+v) \leq I_{k,s}(u) + I_{k,s}(v) \tag{55}$$

When we consider a general solution, since it can be decomposed in a left propagating wave and a right propagating wave and we have, by (55) that $I_{k,s}(u)$ remains bounded if, $I_{k,s}(u^{\pm})$ are finite; here $u^{\pm}$ are the initial conditions given by the D'Alambert solution in (14).

Some of the quantities in (54) have physical meaning – depending on the interpretation of the equation–. On the mathematical side, study of the asymptotic behavior of (54) gives information on the shape of the solutions and has been a customary diagnostic in wave equations.

Remark V.2 *Note that there are other conserved quantities. We could have used* $I(u) = \int_{\mathbb{R}} f(\partial_x u)$ *where* f *is any function. Notably when* $f(s) = \log(s)$, *in some cases* I *can have the interpretation of an entropy. There are also conserved quantities that involve partial derivatives with respect to time and, of course, linear and non-linear combinations of all of the above.*

Notably, the energy of the electromagnetic field considered in detail in Section $IIDVB$ *is a combination of formulas involving the derivatives with respect to position and with respect to time. It is the sum of* $I_{1,2}^2(u)$ *and a similar expression for the derivative with respect to time.*

When the $I_{k,s}$ of the above form satisfy (55)*, the argument used in the study of the evolution of the energy apply word for word (note that for one-directionally propagating waves, the derivatives with respect to time and space are the same up to a sign, so that for these waves it suffices to consider the derivatives with respect to space and them use the decomposition given by D'Alambert solution to estimate, via* (55)*, the values of the quantities. We leave to the reader the formulation of statements.*

Of course, when studying the problem in a cavity, the integral in (54) has to be extended to the domain of the cavity. The quantities $I_{k,s}(u)$ will no longer be conserved (note that in the cavity it is impossible to have waves moving just in one direction and, the boundary conditions generate terms in the evolution).

For the problem of the cavity with periodically moving boundaries, the behavior of these quantities has been studied in [18]. Here, we extend the analysis to the case that the two mirrors are moving quasi-periodically.

Given the fact that (15) gives us explicit solutions in terms of the maps of the torus introduced in Section II E, once we know the asymptotic behavior of the torus map, it will be easy to use (15) to read the asymptotic behavior of the quantities (54).

The results are summarized in the following:

Lemma V.3 *Assume that the torus map associated to the quasiperiodic boundary problem satisfies the conclusions of Theorem III.2 and that the initial conditions are smooth enough. Then, the quantities $I_{k,s}(u)$ remain bounded for all time.*

Consider the situation described by two frequencies. Assume that the torus map associated to the quasiperiodic boundary conditions is in a phase locked region with a uniformly hyperbolic attracting circle $\mathcal{L}^+$ with exponent μ and average transit time T. Assume moreover that the initial conditions are supported in the basin of attraction of the circle and are non-trivial.

Then,

$$I_{k,s}(u(t)) \approx C \exp(-\mu/T(k-1/s)t) \tag{56}$$

Remark V.3 *Note that in particular, the above lemma implies that in the case that we have a contractive attractive circle, the quantities $I_{k,s}$ blow up exponentially when $k-1/s>0$ and decrease exponentially when $k-1/s<0$. Similar conclusions were reached in the periodic* *case by [18]. In the case that $k - 1/s < 0$ we have blow up of $I_{k,s}$ for a generic set of initial conditions since a generic initial condition will have some component in the basin of the attractor. On the other hand, in the case that $k - 1/s > 0$, we cannot guarantee that a generic solution decreases since the support will not be contained in the basin for which Lemma V.3 reaches conclusions.*

Remark V.4 *There is a statement very similar to Lemma V.3 in the case that the the wave equation at the boundary satisfies the Neumann Boundary conditions.*

Note that the main argument in Section V F was the observation that if u satisfies the wave equation with Neumann boundary conditions, then $\partial_x u$ satisfies the equation with the boundary conditions (9), (10). Since, clearly $I_{k-1,s}(\partial_x u) = I_{k,s}(u)$, we obtain that, for the Neumann conditions, $I_{k,s}$ is bounded when the KAM theorem applies. In the case that there is an attractive circle, for initial conditions in the support of the basin we have exponential blow-up when $k + 1 - 1/s < 0$ and exponential decrease when $k + 1 - 1/s > 0$.

The proof of Lemma V.3 is extremely simple. We start by observing that given $\lambda > 1$ the dilated function $\tilde{u}(x) = u(\lambda x)$ satisfies

$$I_{k,s}(\tilde{u}) = \lambda^{k-1/s} I_{k,s}(u) \tag{57}$$

In the system of coordinates x'_n provided in Lemma V.1 we have that denoting $I'_{k,s,n}(u) = \left(\partial^k_{x'_n} u(x'_n, t_n + \Delta)^s\right)^{1/s}$ we have (by (57) and the fact that, in the x'_n coordinates, the characteristics contract by exactly $\exp(\mu)$ in each iteration)

$$I'_{k,s,n}(u) = \exp -\mu n(k - 1/s) I'_{k,s,0} \tag{58}$$

Using the chain rule for derivatives (the Faa-di-Bruno formula) we obtain that

$$\partial^k_x u = \sum_{j=1}^{k} C_{j,n} \partial^j_{x'_n} u \tag{59}$$

where $C_{j,n}$ are algebraic expressions involving only derivatives of x'_n with respect to x. (Very explicit expressions for the C_j can be found, e.g. in [49] p. 42.)

We note that, in particular, all the C_j are bounded independently of n. Moreover $C_k = (\partial_x x'_n)^k$ is bounded from below uniformly in n.

In the case that $k - 1/s < 0$ (exponential divergence) we bound

$$||\sum_{j=1}^{k-1} C_{j,n} \partial^j_{x'_n} u||_{L^s} \leq K \exp(-\mu n(k - 1 - 1/s)) \tag{60}$$

and, using the expression for C_k and that it is bounded away from zero,

$$||C_k \partial^k_{x'_n}||_{L^s} \geq C||\partial^k_{x'_n} u||_{L^s} = \exp(-\mu n(k - 1/s))||\partial^k_{x'_0} u||_{L^s} \tag{61}$$

Note that, by the assumption that the initial condition is non trivial, the right-hand side of (61) is not zero.

Hence, we see that in (59), the term with $j = k$ dominates all of the others and has the desired asymptotic expansion.

To show exponential convergence in the case $k - 1/s > 0$ is even easier since we are only claiming an upper bound that can be obtained by applying Minkowski's inequality to the terms in (59).

H. Two moving mirrors

Our approach can also be easily adapted to describe a situation where the two boundaries of the cavity are moving quasi-periodically. (In particular, if they are moving periodically or stay fixed.)

We assume that the right and left mirrors are moving respectively as $a_R(t) = \Phi_R(\boldsymbol{\omega}^R t)$ $a_L(t) = \Phi_L(\boldsymbol{\omega}^L t)$ where, in a manner analogue as the case of one moving mirror: $\Phi_R : \mathbb{T}^{d_R} \mapsto \mathbb{R}$, $\Phi_L : \mathbb{T}^{d_L} \mapsto \mathbb{R}$, $\boldsymbol{\omega}^R \in \mathbb{R}^{d_R}$, $\boldsymbol{\omega}^R \in \mathbb{R}^{d_R}$.

To ensure that the speed of the mirrors is always smaller than the speed of light and that the cavity does not collapse, we will assume analogously to (4), (4) that

$$|a'_{R,L}(t)| < 1 \tag{62}$$

$$\Phi_R^{\max} \geq a_R(t) \geq a_L(t) + \delta \geq a_L(t) \geq \Phi_L^{\max} \tag{63}$$

The state of the system at a time t can be described by specifying the internal phases of the two mirrors. $\boldsymbol{\xi}_R, \boldsymbol{\xi}_L$ respectively. This phases are evolving in time with velocities $\boldsymbol{\omega}_R, \boldsymbol{\omega}_L$.

As before, we note that if we specify that a characteristic reflects on the right mirror when the internal phases have a certain value, we have specified the evolution of the characteristic.

Hence, to study the characteristics, we will study the variables $\boldsymbol{\xi}^n = (\boldsymbol{\xi}_R^n, \boldsymbol{\xi}_L^n)$ at which the n^{th} reflection with the right mirror takes place. (It goes without saying that we could have chosen just as well the times of reflection on the left mirror. Some of the formulas would change, but the results and the analysis remain unchanged.)

If a characteristic reflects for the n^{th} time in the right mirror at time t_n, we see that the time t'_n of the next reflection in the right is determined by solving

$$a_L(t'_n) = a_R(t'_n) - (t'_n - t_n) \tag{64}$$

After that, the next reflection at the right mirror will be obtained by solving

$$a_R(t_{n+1}) = a_L(t'_n) + (t_{n+1} - t'_n) \tag{65}$$

Note that the condition (62) ensures that the equations (64) and (65) have one unique solution, which furthermore depends smoothly on the times that are the data. We can, therefore, write

$$\begin{aligned} t'_n &= (a_L + \mathrm{Id})^{-1} \circ (a_R + \mathrm{Id})(t_n) \\ t_{n+1} &= (a_R - \mathrm{Id})^{-1} \circ (a_L - \mathrm{Id})(t'_n) \end{aligned}$$

Hence,

$$t_{n+1} = (a_R - \mathrm{Id})^{-1} \circ (a_L - \mathrm{Id}) \circ (a_L + \mathrm{Id})^{-1} \circ (a_R + \mathrm{Id})(t_n) \tag{66}$$

If at the time of the n^{th} reflection on the right, the phases of the mirrors are $\boldsymbol{\xi}^n = (\boldsymbol{\xi}_R^n, \boldsymbol{\xi}_L^n)$, at the time of the $n+1$ reflection on the right, they will be

$$\boldsymbol{\xi}^{n+1} = \boldsymbol{\xi}^n + \Gamma(\boldsymbol{\xi})\boldsymbol{\omega} \tag{67}$$

where $\Gamma(\boldsymbol{\xi}) = t_{n+1} - t_n$ is a function of $\boldsymbol{\xi}$.

By the same argument as we used in Section II, we can study the asymptotic behavior of the characteristics by studying the iterates of the map (67).

One case which is particularly intriguing from the physics point of view and which we think deserves further study is when we have $a_R(t) = a_L(t) + A$. That, is, when the cavity is shaking as a rigid object. In this case, it is still possible to obtain the same phenomena we described before, but one has to take into account that the map (67) is more degenerate than in the previous sections since $\boldsymbol{\omega}_R = \boldsymbol{\omega}_L$ and, hence $\boldsymbol{\omega} = (\boldsymbol{\omega}_R, \boldsymbol{\omega}_L)$ is very resonant. Moreover, the map (67) presents some extra cancellations.

Acknowledgments

The authors would like to thank Prof. À. Haro for help in optimizing some of the programs, and Prof. R. Pérez-Marco for discussions and for supplying [30]. The work of R.L. has been supported by NSF grants. The computations have been carried out in the computer system of the Department of Mathematics of the University of Texas at Austin.

---

[1] J. Dittrich, P. Duclos, and P. Šeba, Phys. Rev. E **49**, 3535 (1994).

[2] C. K. Law, Phys. Rev. Lett. **73**, 1931 (1994).

[3] C. K. Cole and W. C. Schieve, Phys. Rev. A **52**, 4405 (1995).

[4] O. Méplan and C. Gignoux, Phys. Rev. Lett. **76**, 408 (1996).

[5] R. de la Llave and N. P. Petrov, Phys. Rev. E (3) **59**, 6637 (1999).

[6] Y. Wu, K. W. Chan, M.-C. Chu, and P. T. Leung, Phys. Rev. A **59**, 1662 (1999).

[7] V. V. Dodonov, A. B. Klimov, and D. E. Nikonov, J. Math. Phys. **34**, 2742 (1993).

[8] V. V. Dodonov, A. B. Klimov, and D. E. Nikonov, J. Math. Phys. **34**, 3391 (1993).

[9] C. K. Law, Phys. Rev. A **49**, 433 (1994).

[10] C. K. Law, Phys. Rev. A **51**, 2537 (1955).

[11] H. Johnston and S. Sarkar, J. Phys. A **29**, 1741 (1996).

[12] Y. Wu, M.-C. Chu, and P. T. Leung, Phys. Rev. A **59**, 3032 (1999).

[13] M. A. Andreata and V. V. Dodonov, J. Phys. A **33**, 3209 (2000).

[14] J. Cooper, IEEE Trans. Antennas and Propagation **41**, 1365 (1993).

[15] J. Cooper, J. Math. Anal. Appl. **174**, 67 (1993).

[16] M. Yamaguchi, J. Differential Equations **135**, 1 (1997).

[17] M. Yamaguchi, Discrete Contin. Dynam. Systems pp. 303–314 (1998), Dynamical Systems and Differential Equations, Vol. II (Springfield, MO, 1996).

[18] J. Dittrich, P. Duclos, and N. Gonzalez, Rev. Math. Phys. **10**, 925 (1998).

[19] N. Gonzalez, J. Math. Anal. Appl. **228**, 51 (1998).

[20] J. Vano, Ph.D. Thesis, University of Texas (2002).

[21] R. de la Llave and N. Petrov (2002), In progress.

[22] M. Yamaguchi, Preprint, 2001.

[23] L. Rayleigh (J. W. Strutt), Phil. Mag. **3**, 338 (1902).

[24] S. J. Larmor, in *Proceedings of the Fifth International Congress of Mathematicians, Cambridge, 1912* (Cambridge University Press, Cambridge, 1913), vol. 1, pp. 197–216, with and Appendix by T. Levi-Civita, pages 217–220.

[25] T. H. Havelock, Phil. Mag. **47**, 754 (1924).

[26] E. L. Nicolai, Phil. Mag. **49**, 171 (1925).

[27] R. Courant and D. Hilbert, *Methods of Mathematical Physics. Vol. II: Partial differential equations* (Interscience Publ., New York, 1962).

[28] P. R. Garabedian, *Partial Differential Equations* (John Wiley & Sons, New York, 1964).

[29] H. F. Weinberger, *A First Course in Partial Differential Equations with Complex Variables and Transform Methods* (Blaisdell, New York, 1965).

[30] A. J. Cortez, Ph.D. Thesis, University of California (2002).

[31] B. R. Fayad, Ergodic Theory Dynam. Systems **22**, 187 (2002).

[32] A. Windsor, in *Smooth ergodic theory and its applications (Seattle, WA, 1999)* (Amer. Math. Soc., Providence, RI, 2001), pp. 809–824.

[33] P. Walters, *An Introduction to Ergodic Theory* (Springer-Verlag, New York, 1982).

[34] V. I. Arnol′d and A. Avez, *Ergodic Problems of Classical Mechanics* (W. A. Benjamin, New York-Amsterdam, 1968).

[35] C. Baesens, J. Guckenheimer, S. Kim, and R. S. MacKay, Phys. D **49**, 387 (1991).

[36] S. Newhouse, D. Ruelle, and F. Takens, Comm. Math. Phys. **64**, 35 (1978/79).

[37] J.-P. Eckmann, Rev. Mod. Phys. **53**, 643 (1981).

[38] C. Grebogi, E. Ott, and J. A. Yorke, Phys. D **15**, 354 (1985).

[39] E. I. Dinaburg and J. G. Sinaĭ, Funkcional. Anal. i Priložen. **9**, 8 (1975), english translation: Functional Anal. Appl. **9**, 279 (1975).

[40] V. A. Chulaevsky and Y. G. Sinaĭ, Comm. Math. Phys. **125**, 91 (1989).

[41] E. I. Dinaburg, Uspekhi Mat. Nauk **52**, 3 (1997).

[42] H. Broer and C. Simó, Bol. Soc. Brasil. Mat. (N.S.) **29**, 253 (1998).

[43] H. W. Broer, G. B. Huitema, F. Takens, and B. L. J. Braaksma, Mem. Amer. Math. Soc. **83**, viii+175 (1990).

[44] J. Llibre and R. S. MacKay, Ergodic Theory Dynam. Systems **11**, 115 (1991).

[45] A. Katok and B. Hasselblatt, *Introduction to the Modern Theory of Dynamical Systems* (Cam-

bridge University Press, Cambridge, 1995).

[46] J. Kwapisz, Ergodic Theory Dynam. Systems **12**, 333 (1992).

[47] R. de la Llave, in *Smooth Ergodic Theory and Its Applications (Seattle, WA, 1999)* (Amer. Math. Soc., Providence, RI, 2001), pp. 175–292.

[48] W. de Melo and S. van Strien, *One-Dimensional Dynamics* (Springer-Verlag, Berlin, 1993).

[49] M.-R. Herman, Inst. Hautes Études Sci. Publ. Math. pp. 5–233 (1979).

[50] Y. Katznelson and D. Ornstein, Ergodic Theory Dynam. Systems **9**, 643 (1989), ISSN 0143-3857.

[51] O. E. Lanford, III, Phys. D **14**, 403 (1985).

[52] G. Świątek, Comm. Math. Phys. **119**, 109 (1988).

[53] J. Graczyk and G. Świątek, Comm. Math. Phys. **176**, 227 (1996).

[54] J. Moser, Ann. Scuola Norm. Sup. Pisa (3) **20**, 265 (1966).

[55] J. Moser, Ann. Scuola Norm. Sup. Pisa (3) **20**, 499 (1966).

[56] V. I. Arnol'd, *Geometrical Methods in the Theory of Ordinary Differential Equations* (Springer-Verlag, New York, 1988), 2nd ed.

[57] J. Moser, *Stable and Random Motions in Dynamical Systems* (Princeton University Press, Princeton, N. J., 1973).

[58] M. B. Sevryuk, in *Hamiltonian Systems with Three or More Degrees of Freedom (S'Agaró, 1995)* (Kluwer Acad. Publ., Dordrecht, 1999), pp. 568–572.

[59] H. Whitney, Trans. Amer. Math. Soc. **40**, 309 (1936).

[60] V. I. Oseledec, Trudy Moskov. Mat. Obšč. **19**, 179 (1968), English translation: *Trans. Moscow Math. Soc.* **19**, 197 (1968).

[61] D. Ruelle, Inst. Hautes Études Sci. Publ. Math. pp. 27–58 (1979).

[62] L. Barreira and Y. B. Pesin, *Lyapunov Exponents and Smooth Ergodic Theory* (American Mathematical Society, Providence, RI, 2002).

[63] M. W. Hirsch and C. C. Pugh, in *Global Analysis (Proc. Sympos. Pure Math., Vol. XIV, Berkeley, Calif., 1968)* (Amer. Math. Soc., Providence, R.I., 1970), pp. 133–163.

[64] N. Fenichel, Indiana Univ. Math. J. **21**, 193 (1971/1972).

[65] N. Fenichel, Bull. Amer. Math. Soc. **80**, 346 (1974).

[66] O. G. Galkin, J. Nonlinear Sci. **4**, 127 (1994).

[67] I. U. Bronshteĭn and A. Y. Kopanskiĭ, Mat. Issled. pp. 3–11, 177 (1989).

[68] U. Kirchgraber and K. J. Palmer, *Geometry in the Neighborhood of Invariant Manifolds of Maps and Flows and Linearization* (Longman Scientific & Technical, Harlow, 1990).

[69] M. Guysinsky and A. Katok, Math. Res. Lett. **5**, 149 (1998).

[70] G. R. Hall, SIAM J. Math. Anal. **15**, 1075 (1984).

[71] A. M. Davie, Nonlinearity **9**, 421 (1996), ISSN 0951-7715.

[72] W. H. Press, S. A. Teukolsky, W. T. Vetterling, and B. P. Flannery, *Numerical Recipes in C: The Art of Scientific Computing* (Cambridge University Press, Cambridge, 1992), 2nd ed.

[73] R. de la Llave and N. P. Petrov, Experiment. Math. **to appear** (2001).

[74] P. Glendinning, U. Feudel, A. S. Pikovsky, and J. Stark, Phys. D **140**, 227 (2000).

[75] V. I. Arnol′d, Izv. Akad. Nauk SSSR Ser. Mat. **25**, 21 (1961), correction: 28:479–480, 1964; English translation: *Amer. Math. Soc. Transl. (2)*, 46:213–284, 1965.

[76] B. B. Peckham and I. G. Kevrekidis, Nonlinearity **15**, 405 (2002).

[77] G. R. Sell, Arch. Rational Mech. Anal. **69**, 199 (1979).

[78] J. Cooper and H. Koch, J. Funct. Anal. **133**, 301 (1995).